THESIS FOR DEGREE OF DOCTOR OF PHILOSOPHY

Lidar Studies of Tropospheric Aerosols and Clouds

Frans Olofson

The thesis will be defended in English on the 10th of Oct, 2008.

Faculty opponent is Associate Professor Richard L. Collins
Geophysical Institute
University of Alaska, Fairbanks, USA

UNIVERSITY OF GOTHENBURG

Department of Chemistry, Atmospheric Science
University of Gothenburg
Sweden, 2008

Lidar Studies of Tropospheric Aerosols and Clouds

Department of Chemistry

University of Gothenburg

SE-412 96 Göteborg, Sweden

Printed by Geson Hylte Tryck AB, Kungsbacka, Sweden 2008

ISBN 978-91-628-7608-1

Cover Picture: Light scattering from a faint cirrus cloud with Aurora borealis in the background. The picture is taken in Andenes, Norway

Abstract

An improved description of aerosol and cloud processes is a prerequisite for successful prediction of future climate change. The climate on Earth is controlled by the radiation budget, *i.e.* the relation between the radiation going into and out from the atmosphere. Aerosols are said to have two main effects on the climate. The direct effect refers to cooling and warming by reflection of incoming solar radiation and absorption of outgoing thermal radiation, respectively. The indirect effect concerns the ability of aerosols to influence cloud formation and to change the optical and physical properties of clouds. Clouds normally occupy at least 50% of the sky on a global scale. The presence of clouds greatly increases the portion of the solar radiation reflected back to space, but on the other hand clouds may absorb outgoing thermal radiation from Earth and in the same way as a greenhouse gas partly counteract the cooling effect. The Intergovernmental Panel on Climate Change has identified clouds as the key uncertainty in predicting climate change: "The single largest uncertainty in determining the climate sensitivity to either natural or anthropogenic changes is clouds and their effects on radiation and their role in the hydrological cycle".

The overall aim of the present thesis is to contribute to an increased understanding of climate effects as well as air quality issues related to aerosol and clouds. The radiative properties of clouds are determined by the microphysics, *i.e.* refractive index, shape, and size distribution. In this thesis the construction and development of a bistatic lidar set-up for polarisation measurements throughout the troposphere is described and the results obtained with this system are presented. From the measurements of optically thin or mildly opaque high latitude clouds substantial depolarisation was observed. Ray tracing calculations for hexagonal ice columns were able to produce all the experimental values if a suitable degree of surface roughness was introduced. The results show that it is important to account for non-spherical shapes for the assessment of the radiative impact of Arctic ice clouds, and that the bistatic lidar technique may provide a useful complementary technique to be used together with existing lidar setups.

Lidar measurements were also conducted with the aim to study particulate air pollution in Göteborg. The limited insolation in wintertime sometimes resulted in near neutral boundary layer conditions and inefficient ventilation during the day. Considerable variation in the rate of rising polluted air subsequent to inversion layer break-up was observed, ranging from 200 to 800 m/h. Recently formed particles were observed around midday subsequent to surface layer ventilation. The boundary layer dynamics are concluded to have a strong impact on the properties of the urban aerosol and to a large extent determine the severity of the wintertime urban air pollution episodes to human health.

Keywords: lidar, bistatic lidar, troposphere, aerosols, clouds, cirrus, ice particles, polarisation, particle shape, CABLE, urban air quality, temperature inversion, dispersion, GÖTE

List of Papers

This thesis is based on the work presented in the following papers:

I. Janhäll, S., Olofson, K. F. G., Andersson, P. U., Pettersson, J. B. C. and Hallquist, M., "Evolution of the urban aerosol during winter temperature inversion episodes", Atm. Environ. **40**, 5355-5366 (2006)

II. Olofson, K. F. G., Andersson, P. U.,Hallquist, M.,Ljungström, E., Tang, L., Chen, D. and Pettersson, J. B. C., "Urban aerosol evolution and particle formation during wintertime temperature inversions", *accepted for publication in* Atm. Environ. (2008)

III. Olofson, K. F. G., Witt, G. and Pettersson, J. B. C., "Bistatic lidar measurements of clouds in the Nordic Arctic region", Appl. Opt. **47**, 4777-4786 (2008)

IV. Olofson, K. F. G., Svensson, E. A., Witt, G. and Pettersson, J. B. C., "Arctic aerosol and clouds studied by bistatic lidar technique", *submitted to* J. Geophys. Res.-Atmos. (2008)

Contents

1 Introduction

Light is scattered by everything coming in its way, for example a wall, a cloud, smoke or molecules in the air. It is the scattered light reaching our eyes that makes us see what we are looking at. Another way to put it is if there were no light scattering we would not see anything else but direct light sources. In the atmosphere suspended particles are responsible for many spectacular optical effects, such as rainbows, red sunsets and halos around the sun or moon. Many optical measurement methods rely on the scattering of light, one of these is lidar.

In this thesis the construction and development of a lidar set-up is described and the results obtained with this system are presented. The applications of the lidar system and the scientific interest have been concentrated to tropospheric aerosols and clouds. The measurements have been conducted on field campaign basis at the Department of Chemistry, University of Gothenburg and at Andøya Rocket Range and ALOMAR (Arctic Lidar Observatory for Middle Atmosphere Research), Norway.

Aerosol particles affect the environment in several ways. The research presented in this thesis is related to two of them, air quality and climate impact. Aerosol particles are always present to smaller or larger degree and are constantly inhaled. A fraction of these particles deposit in the lungs and may pose a threat to human health (Dockery *et al.*, 1993; Pope *et al.*, 1995; Pope *et al.*, 2002; WHO, 2005). The effects are often particularly pronounced during temperature inversion episodes. The climatic influence from aerosols can be divided into two main effects, the direct and the indirect effect (Liou, 2002). The direct effect involves the reflection of incoming sunlight back to space (cooling) and the absorption of outgoing thermal radiation (warming). In addition, aerosol particles have the ability to influence cloud formation and to change the optical and physical properties of clouds (Liou, 2002). Clouds do in turn have a significant although not yet completely understood impact on the magnitude of incoming and outgoing radiation, *i.e.* the radiation budget. These effects are referred to as the indirect effect. Of the different cloud types occurring in the atmosphere cirrus clouds are main responsible for the coverage, with a global average of 20 – 30 % (Liou *et al.*, 1986; Wylie *et al.*, 1994).

The research projects presented in this thesis are based on four appended papers related to the field campaigns. These are:

- The GÖTE campaigns performed in Göteborg, dealing with urban air quality and boundary layer aerosol dynamics (paper I and II).

- The CABLE campaign performed in Northern Norway, dealing with high latitude clouds with emphasis on ice clouds and particle shape (paper III and IV).

The GÖTE campaigns were a joint effort with several participating groups investigating the Göteborg urban air quality. The CABLE campaign was carried out in cooperation with a lidar observatory with the purpose to implement and explore the capabilities of a newly developed lidar system.

This introduction is followed by a description of aerosol properties and their role in the atmosphere in Chapter 2. Chapter 3 presents the lidar technique and gives an

introduction to atmospheric light scattering theory. The description of the lidar set-up that was constructed is given in Chapter 4, together with the data analysis procedure. In Chapter 5 results and conclusions from the measurements are presented. Finally, some concluding remarks and an outlook for future work is given in Chapter 6.

2 Background

2.1 Aerosols

The word aerosol refers to a two-phase system and is defined as solid or liquid particles suspended in a gas, normally air. The sizes of the particles range from roughly 1 nm up to more than 100 μm. The residence time of an aerosol particle in the atmosphere can extend up to weeks or in extreme cases a year or more (Hinds, 1999). The smallest particles lie on the boundary to molecular or atomic clusters and the lifetime is limited by break-up or coagulation with other particles, while for the big particles it is the deposition rate that limits the lifetime.

The sources of aerosols are many and the nature of the aerosols is therefore greatly varied. Some of the most abundant aerosol types are wind generated sea spray and mineral dust, clouds, biogenic aerosols (*e.g.* spores and pollen) and soot from fossil fuel and biomass burning. Aerosol particles can also arise in the form of so-called secondary aerosols through gas-to-particle conversion. Examples of this are particles consisting of sulphate formed from sulphur dioxide oxidation in cloud droplets, particles formed *via* condensation of hot gases emitted during combustion and particles generated from oxidation of low vapour pressure organics released from vegetation.

Aerosols can affect the environment and climate in several ways. Particles scatter sunlight and may also absorb thermal radiation from Earth. In addition, particles influence the cloud formation and properties. These effects are important factors influencing the climate. Also plants and animals, including humans, are affected. Deposition of particles will distribute chemicals which can lead to altering of ecological systems. The deposition of potentially toxic substances and the presence of the particles themselves in the lungs are thought to act harmful to human health. Another important role of the aerosols in the atmosphere is to provide sites for chemical reactions. Many small particles have a large available surface area for surface reactions to take place. In liquid particles, like cloud droplets, reactions may take place in the bulk phase.

The concentration of particles is very different depending on environment. In the very cleanest environment on Antarctica the concentration can be as low as 1 – 10 particles/cm^3 while in the other extreme, *e.g.* close to industries or heavily trafficked roads, as high concentrations as 10^7 – 10^8 particles/cm^3 can be found (Seinfeld & Pandis, 1998).

The number concentration concept is a good way to represent the smaller particles. Another, more common, way to indicate the aerosol concentration is by the mass of the particles. Mass concentrations are reported in terms of PM_{10} and $PM_{2.5}$, which are the particulate mass per air volume of particles with diameter less than 10 and 2.5 μm, respectively. For extremely polluted or dusty areas the PM_{10} levels can be as high as 1 mg/m^3 but for urban areas the concentrations are typically one to two orders of magnitude lower. The PM concept mainly accounts for large particles. As an example, the mass of a 10 μm particle is equivalent to the mass of one billion 10 nm particles. For this reason mass concentration is suitable in situations where deposition is

important. In other situations the number concentration is a more suitable way to represent the aerosol loading, *e.g.* when discussing the effects on clouds.

Concerning the mass of emitted aerosol particles, natural sources greatly exceeds the emissions from anthropogenic sources, estimated to 3100 and 450 Tg/y, respectively (Seinfeld & Pandis, 1998). Anthropogenic aerosols to a high degree consist of small particles while natural aerosols generally are emitted as big particles. Although lower in mass, anthropogenic aerosols often play a more important and widespread role in environmental influence of the atmosphere.

The aerosol size spectrum is traditionally divided into regions based on typical mass distributions (Fig. 1). Particles are divided into fine and coarse, between which the limit has been set to a particle diameter of 2.5 μm. This is roughly the size below which particles starts to follow the inhaled air far enough down the respiratory system, *i.e.* into the lungs, to be harmful for our health. The further down in the lungs the particles are deposited the more harmful they may act. Coarse particles on the other hand do not so easily follow the air flow but are deposited early in the respiratory system and then removed from the body with mucus. The fine particles are divided into two modes, the nuclei or Aitken mode ($d \leq 0.1$ μm) and the accumulation mode ($0.1 \leq d \leq 2.5$ μm). The nucleation mode particles form from homogenous nucleation and gas-to-particle conversion. The particles in this size mode are short lived. The small sizes make them very mobile resulting in a rapid coagulation which together with condensation of low volatility vapours result in the formation of bigger particles eventually ending up in the accumulation mode. The mode is so called because there are no effective removal processes for this size range. The particles are too small to undergo any effective sedimentation and too big for coagulation to be effective, and the mode is constantly filled by accumulation of coagulating nuclei mode particles. As indicated in Fig. 1 the only effective, although slow, deposition processes for the accumulation mode are rainout and washout. Rainout which is most efficient for the smaller particles in the mode is the process where particles are removed by incorporation into cloud droplets. The bigger particles in the accumulation mode can be trapped by falling rain drops and by this way removed from the atmosphere in what is called washout.

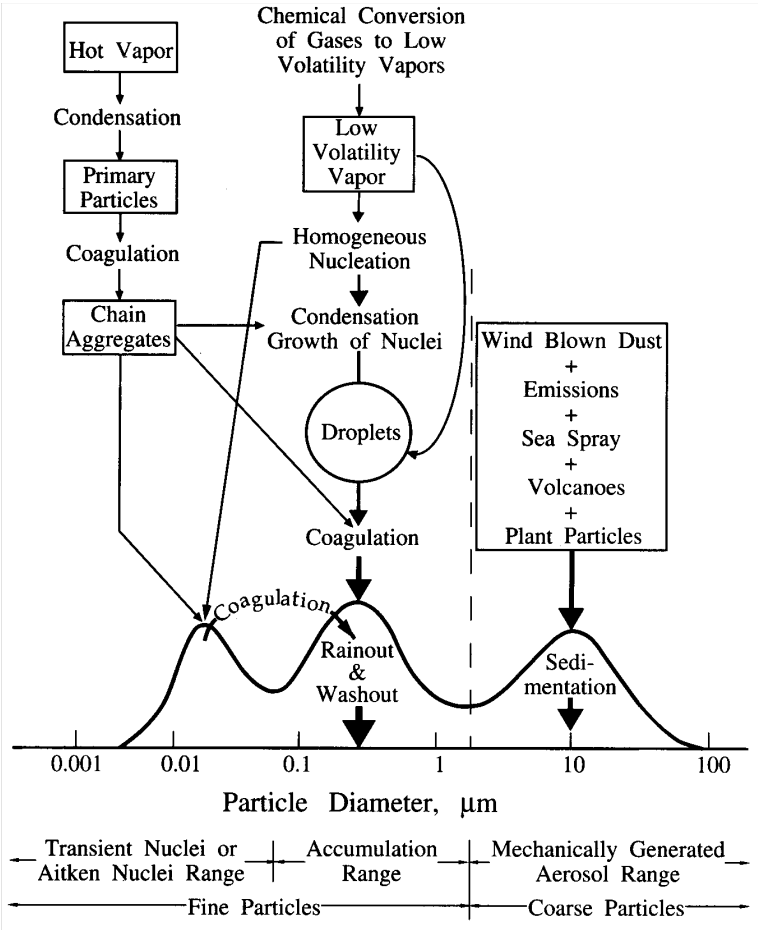

Fig. 1 Overview of aerosol size classification together with main sources and sinks. (source: *Atmospheric Physics and Chemistry*, Seinfeld & Pandis, 1998)

2.2 Boundary Layer Processes

The troposphere can be divided into two parts, the boundary layer (or more correctly, the planetary boundary layer, PBL) and the free troposphere. The boundary layer is directly influenced, *i.e.* in an hour or less, by the presence of the Earth's surface and responds rapidly to forcings such as solar heating, evaporation and transpiration, frictional drag and terrain-induced flow modification. These forcings generates turbulence, keeping this part of the atmosphere well mixed (Stull, 1988). The top of the PBL is associated with the lifting condensation level at which moist air becomes saturated and starts to condensate. This may introduce a region of increasing temperature giving a so-called capping inversion (Fig. 2).

2.2.1 Temperature Inversion

The most important factor determining the boundary layer height during daytime is the magnitude of the convective heating (Seinfeld & Pandis, 1998). From lidar measurements in Göteborg it was established that the typical daytime boundary layer height during winter time is typically around 1 km (Janhäll *et al.* 2006; Olofson *et al.*, 2008). When the sun is setting the convection gradually decreases and finally ceases. At this point the radiative cooling of the ground becomes the dominant process of heat exchange. Since the ground is a much more effective radiator than the air above, the

ground temperature decreases faster resulting in a positive temperature gradient. This is what is called temperature inversion. The result is an inversion layer near the ground in which the air is prevented from rising (Fig. 2). The layer is also called stable boundary layer, referring to the prevented mixing therein. For a temperature inversion to be able to arise the radiative cooling should be effective, *i.e.* absence of clouds and the wind speed should be low. The situation can be further enhanced if the area is surrounded by mountains and in river valleys because of downward transportation of cold air. Göteborg is an example where such circumstances can influence the atmospheric stability (Holmer & Haeger-Eugensson, 1999). When the sun rises in the morning the ground is heated shifting the temperature gradient to negative which breaks up the inversion. The trapped air is then released and mixing with the air left above from the day before, the so-called residual layer, takes place.

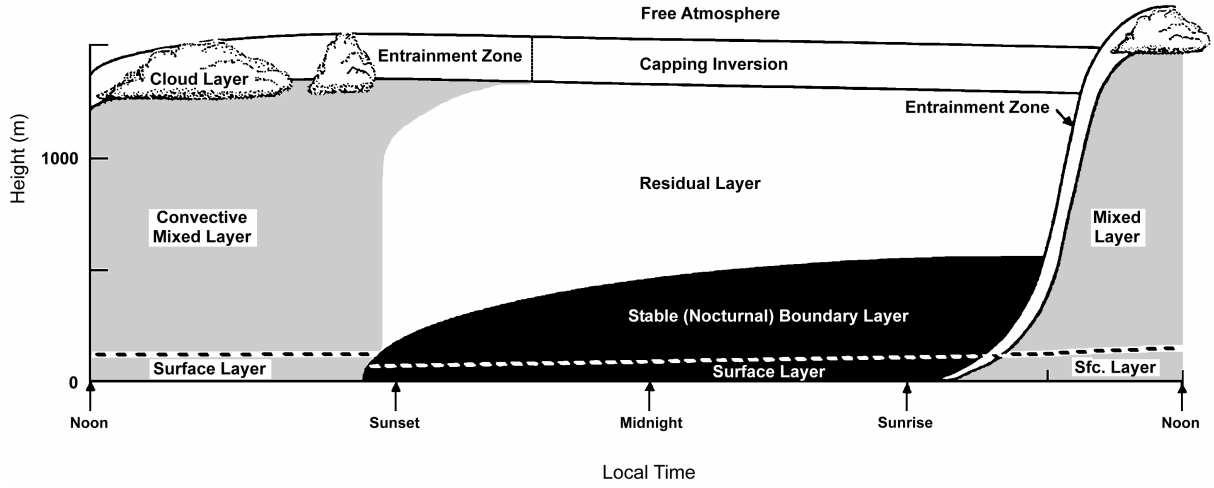

Fig. 2 The boundary layer with its three main types of sub-layers, the turbulent mixed layer, the less turbulent residual layer containing the former mixed layer air and the stable inversion layer. (adapted from *An Introduction to Boundary Layer Meteorology*, Stull, 1988)

2.2.2 Health Effects

Air pollution in the form of aerosol particles has been shown in several studies to have negative effects on human health (Dockery *et al.*, 1993; Pope *et al.*, 1995; Pope *et al.*, 2002; WHO, 2005). Most of the health studies concerning aerosol particles are focused on the PM_{10} and $PM_{2.5}$, for which $PM_{2.5}$ generally seems to have a more clear association with health effects (Pope & Dockery, 2006). However, smaller particles, in the accumulation and nuclei modes, which due to their low mass do not influence mass concentrations to a large extent are also thought to be of great concern. Coarse particles are likely to be retained in the nasal and oral cavities, whereas the more mobile fine particles are likely to reach the lungs and be retained there. The walls of the lungs are covered with something similar to tiny hairs, called cilia, and a layer of mucus (Hinds, 1999). The particles that impact in the mucus are by a constant cilia motion transported up through the lungs and then end up down in the gastrointestinal tract. The smallest particles in the nuclei mode, smaller than 10 nm, undergo efficient diffusion and therefore get stuck throughout the respiratory system. On the other hand, the diffusion of the somewhat bigger particles in the upper nuclei mode and lower accumulation mode, roughly between 10 and 100 nm, is not very effective but the particles are still small enough to follow the air stream down the respiratory system. The effect is deposition of particles in this size range at the very

end of the microscopic lung branches, *i.e.* the alveoli. It is the alveolar region that is responsible for the oxygen exchange and therefore there is no protective mucus layer and no cilia. The result is inefficient clearance and thus deposited particles are thought to cause inflammatory response, and if dissolved also possible toxic responses. The role of deposition in the alveoli are, however, still unclear.

2.3 Climate

The climate on Earth is controlled by the radiation budget, *i.e.* the relation between the radiation going into and out from the atmosphere, respectively (Fig. 3). The source behind the energy cycle is the solar radiation, in this context referred to as shortwave radiation. The effect of the solar radiation is heating of Earth and the atmosphere covering it. Since the Earth is heated it also exchanges energy by longwave heat radiation. Much of the incoming radiation is absorbed by the atmosphere and about one third escapes back to space by reflection by the atmosphere, clouds and aerosols and by the Earth's surface. The reflected portion is called the planetary albedo and is responsible for reduced heating of the Earth. In addition, the land surface, oceans, clouds and the atmosphere itself absorb and emit their own radiation. After successive absorption and emission the other two thirds of the incoming solar energy, not directly reflected, leaves the atmosphere as outgoing longwave radiation. The ability to emit decreases with decreasing temperature. When the atmosphere absorbs energy emitted from the Earth's surface the absorbed emission is replaced by the atmosphere's own emission. Since the atmosphere generally has a lower temperature than the Earth's surface the amount of re-emitted longwave radiation is smaller than the amount absorbed. The result is a decrease of the energy escaping out to space and hence a warming of the atmosphere, *i.e.* the process known as the green house effect.

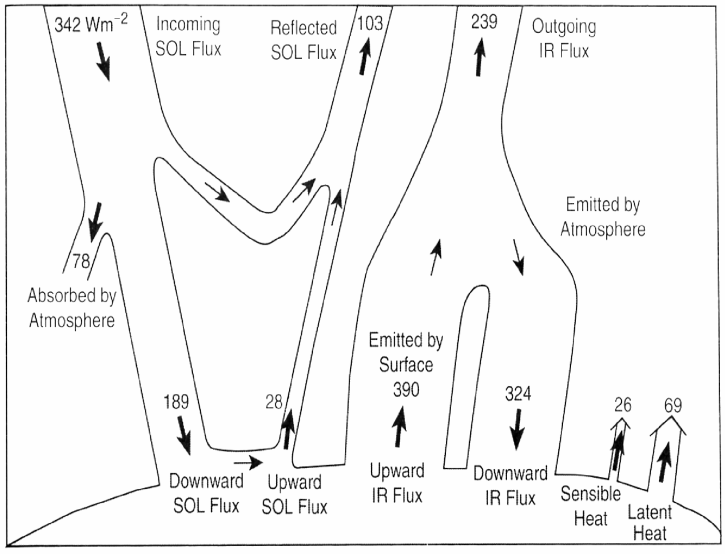

Fig. 3 The radiation budget of Earth and its different components and their proportions. The sketch is based on a planetary albedo of 30% and a ground temperature of 288 K. (source: *An Introduction to Atmospheric Radiation*, Liou, 2002)

Aerosols are said to have two main effects on the climate. The *direct effect* refers to cooling and warming by reflection of incoming solar radiation and absorption of outgoing heat radiation. The *indirect effect* deals with the ability of aerosols to

influence cloud formation and to change the optical and physical properties of clouds. Increasing the number of particles while keeping the water content unchanged will increase the number of cloud particles and decrease their size, which in turn prolongs the cloud lifetime and coverage. The magnitude of the effects on climate for aerosols are quite uncertain, this is especially true for the cloud indirect effect (IPCC Fourth Assessment Report (AR4), 2007).

2.3.1 Clouds

Aerosols and clouds are known to have a significant impact on the climate. The average net effect is cooling but the uncertainties are quite large and the magnitude of the forcing shows large differences globally (IPCC Fourth Assessment Report (AR4), 2007). The presence of clouds greatly increases the portion of the solar radiation reflected back to space (*solar albedo effect*) but on the other hand clouds absorb outgoing thermal radiation from Earth and in the same way as a greenhouse gas partly counteract the cooling effect (*infrared greenhouse effect*). Clouds normally occupy at least 50% of the sky on a global scale (Liou, 2002) and the cloud type main responsible for the coverage is cirrus clouds, which are present at all latitudes and during the whole year with an average global coverage of 20 – 30 % (Liou *et al.*, 1986; Wylie *et al.*, 1994). Cirrus, defined as high clouds, consisting of ice and generally stable and long lived (Liou, 1986), are known to contribute to the infrared greenhouse effect (Liou, 2002). The relatively large ice particles, ~µm – mm (Heymsfield *et al.*, 1990; Liou & Takano, 2002), to a large extent scatter the shortwave sunlight into the forward direction acting transparent. The longwave radiation from Earth on the other hand is effectively absorbed by the ice and reradiated at the high altitude low cloud temperature. Because of the curvature of the Earth most of the solar energy is received around the equator and distributed towards the poles. The thermal radiation from Earth is only dependent on the Earth's temperature resulting in a negative net radiative flux at high latitudes. This makes the polar regions particularly sensitive to the IR greenhouse effect exerted by cirrus.

3 The Lidar Technique

The LIDAR (LIght Detection And Ranging) technique is a widely used method for remote sensing of the atmosphere, which can give vertical profiles of molecular density and aerosols as well as atmospheric features like clouds. The first reported atmospheric applications of lidar concerned detection of aerosol layers were performed by Fiocco and co-workers (Fiocco & Smullin, 1963; Fiocco & Grams, 1964). Using a similar laser source, Witt and Lundin (1971) performed high-altitude soundings in an attempt to detect scattering from noctilucent clouds in the 80-84 km altitude region. The basis for the lidar technique is to illuminate the atmosphere with electromagnetic radiation (light) and then collect the part of the emitted light which is scattered back to a receiver. For this a pulsed laser is used. The intense light gives the opportunity to record signal from high altitudes, which depending on the interest of research and type of equipment means an upper limit from a couple of km up to around 100 km. The laser is normally vertically directed and since it is pulsed it is possible to obtain a vertical profile. The early lidar set-ups were based on the Ruby laser. Nowadays the Nd:YAG laser is by far the most widely used type. Other types include the dye laser for resonance scattering measurements, *e.g.* sodium, and excimer laser for ozone concentration measurements. The Nd:YAG laser is in principal used for three types of applications related to type of light scattering, Rayleigh, Mie and Raman scattering. The elastic Rayleigh scattering is used for atmospheric density measurements. The Lorenz-Mie scattering arises from the interaction with aerosols. This type of lidar application is basically used for the purpose of two properties, aerosol concentration if more than one wavelength is analysed and particle shape if the polarisation state is characterised. In both cases assumptions have to be made. The Raman lidar also have two main applications, vibrational and rotational Raman scattering. The vibrational Raman shift can be utilised for measurements of atmospheric constituents, *e.g.* water, while the rotational Raman can give the local temperature (Kovalev & Eichinger, 2004).

The lidar measurement begins as the laser pulse leaves the laser and simultaneously a clock is started. The time in the scan is related to the altitude from which the collected light is scattered, via $h = ct/2$, where h is altitude, c is the speed of light and t is the time in the measurement scan. The fact that the light has to travel up to the scattering volume and back down to the receiver is reflected by the 2 in the denominator. The highest possible range resolution is ultimately restricted by the laser pulse length, which for the commonly used Nd:YAG laser is on the order of 5 to 10 ns, corresponding to 0.75 to 1.5 m. However, the range resolution can be limited by the sampling rate of the electronics. The receiver is made up by a telescope which focuses the scattered light onto a photo sensitive detector. The telescope is often constructed for measurements from several km which means that scattering from the very first part of the atmosphere will not be accurately collected. The altitude above which the receiver's field of view (FOV) overlaps the laser beam and proper collection is achieved is normally a couple of hundred metres. However, if the lidar is optimised for high altitude measurements the lower limit for which signal is recorded can be limited to several kilometres due to too high signal close to ground. For the visible part of the electromagnetic spectrum a photomultiplier (PM) is used. The PM converts light into a current which can be measured electronically. Because of a very rapid decrease in the signal with increasing scattering altitude, a very large dynamical range in the signal is a necessary requirement. This puts demands on the signal processing. In the

beginning of the scan the signal is high and analogue recording of the PM current is normally adopted, while in the end of the scan where the signal is several orders of magnitude lower photon counting is suitable to achieve an acceptable signal-to-noise (S/N) ratio. The best possible time resolution corresponds to one measurement scan for every laser pulse, in the case for the Nd:YAG laser in the order of 0.05 s. However, this will give too noisy signal and in practice time averaging is used resulting in typical time resolutions ranging from a minute up to an hour, depending on which altitude regime is of interest. Enhanced S/N ratio is also achieved by means of averaging over altitude in the scan, resulting in decreased range resolution (Kovalev & Eichinger, 2004).

3.1 Light Scattering in the Atmosphere

As mentioned above, the concept of the lidar technique is to measure to which extent electromagnetic radiation is scattered in the atmosphere through interaction with present scatterers, *i.e.* molecules and particles. There are different scattering regimes depending on the relationship between the size of the scattering object and the wavelength of the radiation. For lidar measurements the radiation utilised is normally confined to the visible or close to the visible part of the electromagnetic spectrum. In the process of scattering the light interacts with the scattering object under which standing waves and electrical fields are induced. These electrical fields then reradiate their energy. The magnitude and angular pattern depend on the nature, *i.e.* size, refractive index and shape, of the scattering object or particle. When the size of the particle is much smaller than the wavelength of the incident light, *i.e.* the size parameter, $x = \pi d/\lambda << 1$ (van de Hulst, 1957), as is the case with the air molecules, the scattering is called Rayleigh scattering. Figure 4 illustrates the scattering pattern with the two polarisation components I_1 perpendicular and I_2 parallel to the scattering plane. The scattering plane is defined by the direction of the incoming and outgoing light forming the scattering angle, θ. The total intensity of the scattered light is obtained as $I_1 + I_2$.

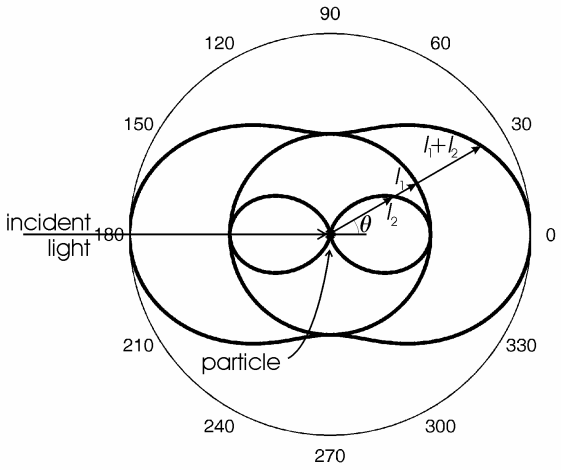

Fig. 4 Polar plot of Rayleigh scattered randomly polarised light. I_1 and I_2 are the two polarisation components, oriented perpendicular and parallel to the scattering plane.

The term Rayleigh scattering is by strict definition restricted to scattering of light in the atmosphere. The nature of this type of scattering has the character of dipole

scattering, which it closely resembles but to a small degree deviates from due to the slight anisotropy of the elongated nitrogen and oxygen molecules in the air. One feature of Rayleigh scattering is to give the sky its blue colour. The reason for this is that the scattering efficiency is inversely proportional to the fourth power of the wavelength, hence being most effective in the blue end of the white sunlight spectrum.

The Rayleigh or dipole scattering is the small-particle limit approximation of the general type of scattering called Lorenz-Mie scattering. The Lorenz-Mie theory is based on Maxwell's equations and can be used to find the exact solution to the scattering problem for spherical particles with arbitrary sizes, *i.e.* also for particles comparable to or larger than the wavelength (van de Hulst, 1957). One important example of such particles is cloud water droplets. This type of scattering gives far more complex scattering patterns than the Rayleigh scattering. An example of such a pattern is shown in Fig. 5 in which the phase function is characterised by large and rapid oscillations that can range several orders of magnitude. This structure is traditionally explained as the result of interference of light diffracted and transmitted by the particles. As the particle size increases the oscillations grow larger and the interference maxima and minima occurrences approach smaller and smaller angular intervals. In addition to the large scale interference structure there is a superimposed small scale ripple which is caused by resonance effects from light waves propagating along the particle surface boundary through internal reflections. The discussion about the oscillating nature of the phase function holds for a single scattering particle or a monodisperse aerosol. However, in the atmosphere aerosols are polydisperse and the structured features are partly averaged out. As the width of the size distribution increases the oscillations becomes less pronounced and the resonance ripple disappears accompanied by a smoothed interference structure (van de Hulst, 1957; Bohren & Huffman, 1998; Mishchenko *et al.*, 2005). A common characteristic for scattering by particles large enough to fall outside the Rayleigh regime is the strong enhancement of scattered light in the forward direction. The reason for this feature can be thought of as a result of two contributions; light reflected twice inside the particle continuing in the forward direction and light diffracted into the forward direction.

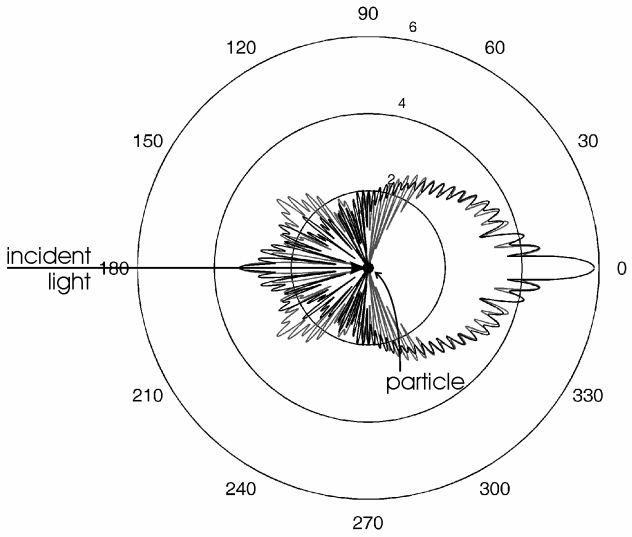

Fig. 5 Polar plot of the scattering from a 7 μm water droplet for 532 nm randomly polarised light (perpendicular polarised component, I_1: black solid line; parallel polarised component, I_2: grey solid line). The indicated intensity scale is logarithmic, with a base of 10.

As the particles grow even larger so that the size is much larger than the wavelength, a new scattering regime is entered in which the calculations are simplified by the fact that the light can be considered consisting of separate rays that undergo reflection and refraction at the particle surface. Thus, in this regime geometric optics can be used to find the scattering properties of the particles. The fundamental upon which this scattering regime is built is Snell's law

$$m_1 \sin\theta_1 = m_2 \sin\theta_2 , \qquad (1)$$

which gives the relationship between angles of incidence, θ_1 and refraction, θ_2 for a wave impinging on an interface between two media with different indices of refraction, m_1 and m_2. A critical size parameter above which it is acceptable to use geometric optics is difficult to set. Depending on what kind of scattering feature, *e.g.* the rainbow, is of interest the lower limit of x is somewhere in the range 50 – 400 (Liou & Hansen, 1971).

3.2 The Lidar Equation

The fundamental tool to extract the inherent information in the scattered light collected by the telescope is the lidar equation. In this equation the received energy or intensity is related to the emitted through the radiative properties of the scattering volume and the beam path. The lidar equation is

$$I(h) = CI_0 \frac{\Delta h}{h^2} \beta(h) e^{-2\int_0^h \alpha(h')dh'} . \qquad (2)$$

I(h) is the received intensity from altitude h and I_0 is the emitted intensity. To obtain the vertical profile the measurement is divided into short (typically in the order of ns) consecutive time intervals, each corresponding to an altitude. $\Delta h = c\tau/2$ is the height interval responsible for the scattered return where c is the speed of light and τ is the time interval during which the signal is measured. In order to correct for the decreasing scattering cone seen by the telescope as the scattering altitude increases the square of the altitude, h^2 is inserted in the denominator. $\beta(h)$ is the backscattering coefficient at altitude h. The laser light is attenuated first on the way up to the scattering volume and then on the way down to the receiver. This exponential decay, called the two-way transmittance, is expressed in the last term where the extinction coefficient, $\alpha(h')$ is integrated twice over the interval from ground to the scattering altitude, h. The constant C is related to the instrument and includes receiver area and receiver efficiency. C, β and α are functions also of wavelength but in this work only 532 nm has been used. The parameters in the equation containing the information about the atmosphere are the *extinction coefficient* and the *backscattering coefficient*. The extinction coefficient describes to which extent the emitted laser light is lost on its way up to the scattering object and back down to the telescope. This loss is due to scattering in other directions than the 180° backscattering direction and to any possible absorption. The differential backscattering coefficient gives the relation of the amount of scattered light in the direction of interest and that of the incident light. Both the extinction and backscattering coefficients can be separated into a molecular and particulate contribution.

3.3 Signal Inversion

In the received signal there is a constantly present but varying background signal. The sources for the background are mainly ambient light, especially during daytime, and photomultiplier dark current, *i.e.* the spontaneous emission of electrons from the photo cathode. If the length of the measurement scan is chosen long, so that the end of it corresponds to altitudes where the laser light has become totally attenuated, any signal in this part of the profile represents the background. By taking the mean in some region in this part the removal of the background contribution can be conveniently done by subtracting the full profile with this mean value. Since the background generally fluctuates the removal should be done separately for each profile in a set of several consecutive collected profiles. An alternative method for background subtraction is to measure the signal without laser light before and/or after the lidar measurement.

The desired quantities in the lidar equations are α and β. They can be resolved into their molecular and aerosol origin, respectively, and treated as arising from two different independent scattering contributions, *i.e.*

$$\alpha(h) = \alpha_m(h) + \alpha_a(h) \text{ and} \tag{3}$$

$$\beta(h) = \beta_m(h) + \beta_a(h), \tag{4}$$

where *m* stands for molecular and *a* for aerosol.

α_m and β_m may be theoretically determined from Rayleigh theory if the temperature and pressure profiles are available from soundings, or assumed by means of a standard atmosphere. Left to determine is the aerosol optical parameters $\alpha_a(h)$ and $\beta_a(h)$. However, a problem arises; there are two unknown but only one equation. A range of solutions, often with several different variations, to this problem has been suggested. Below, two common ways to process the lidar data will be presented.

3.3.1 The Klett/Fernald Algorithm

To retrieve profiles of the extinction and backscattering coefficients probably the most widely used strategy for the lidar equation inversion is to define some analytical relation between α and β. The solutions based on this concept stem from radar analysis of rain-fall. For lidar purposes a stable solution for a single-component turbid atmosphere, *i.e.* when the aerosol scattering contribution dominates, was formulated by Kaul (1977) and Klett (1981) independently, but has become known as the Klett's far-end solution or the Klett algorithm. Later Fernald (1984) reformulated the solution for the two-component atmosphere case and hence to the general form which has gained widespread use today.

In the formulation by Klett the relationship between α and β is formulated by

$$\beta = c\alpha^k. \tag{5}$$

In Klett (1981) it was stated that indications showed "that great accuracy in the determination of k is not required" and k is often set to unity (for single scattering conditions) giving a simple linear relationship. As discussed above α and β can be resolved into a molecular and an aerosol component. The theoretical value for $S_m = \alpha_m/\beta_m$ in the 180° backscattering direction (or 0° forward direction) calculated from Rayleigh theory is $8\pi/3$ sr, under the condition of zero molecular absorption. The particulate equivalence is called aerosol extinction-to-backscatter ratio, $S_a = \alpha_a/\beta_a$ and when $k = 1$ holds, $S = 1/c$.

In the solution of Fernald an inward stepwise integration is performed from some altitude h_2 down to some altitude h_1 in steps of Δh. The solution for the extinction coefficient at the altitude, $h - \Delta h$ one step below the proceeding altitude, h above is

$$\alpha_a(h-\Delta h) = \frac{X(h-\Delta h)e^{A(h-\Delta h,h)}}{\frac{X(h)}{\alpha_a(h)+S_a/S_m\alpha_m(h)} + \left(X(h)+X(h-\Delta h)e^{A(h-\Delta h,h)}\right)\Delta h} - \frac{S_a}{S_m}\alpha_m(h-\Delta h) \quad (6)$$

where $X = I(h)h^2$ is the range corrected signal and $A(h - \Delta h,h) = (S_a - S_m)(\beta(h - \Delta h) + \beta(h))\Delta h$. A calibration altitude h_r somewhere within this interval is chosen at which the extinction coefficient is known or assumed. The choice of h_r at the upper end of the integration interval together with downward integration, responsible for the notation far-end (boundary point) solution, has shown to give a more stable inversion, at least in turbid atmospheres (Fernald, 1984; Kovalev & Eichinger, 2004). Furthermore, with this strategy one can choose h_r high enough that the aerosol contribution to the extinction can be considered small and approximated to zero. In this case and if h_r coincides with the upper starting altitude α_a is zero in the first step of the integration and left to define before the integration can start is S_a. For aerosols, the relationship between the backscattering and the extinction depends, except for the laser wavelength, on the aerosol microphysics, *i.e.* refractive index, shape, and size distribution. In real atmospheres, both α_a and β_a may vary over a wide range, while the aerosol extinction-to-backscatter ratio varies over a much smaller range, most typically by a factor of 5 – 10 (clouds excluded), and the variations are in addition smooth (Kovalev & Eichinger, 2004). The assumption of a constant S_a is therefore a reasonable good approximation in well mixed regions of the atmosphere. The choice of an appropriate value for S_a has been widely discussed and depends on the atmospheric nature in question. Kovalev & Eichinger (2004) do in their book present values reported from a wide range of measurements, ranging from 10 up to almost 80 sr. However, the importance of the start value decreases with increasing aerosol load and in the limit of the single-component case of Klett no aerosol extinction-to-backscatter ratio is needed (Fernald, 1984). The Klett algorithm is best suited in cases of (very) high extinction, such as dense fog or clouds, whereas the Fernald algorithm is better suited for thinner clouds.

3.3.2 Range Corrected Signal

It is common to present lidar data as range-corrected signal (RCS), *i.e.* the received signal multiplied by h^2 described above. In molecular atmospheres or atmospheres with low aerosol content the RCS plotted on a logarithmic scale will fall off close to linearly, reflecting the decrease in molecular density. In well mixed, aerosol containing atmospheres the attenuation is mostly due to particulate extinction and the linear fall-

off is the basis for the slope method to determine the average atmospheric extinction (Kovalev & Eichinger, 2004). Any additional features in the profile are a result of more rapid changes in the aerosol loading and the use of the RCS is a convenient way to detect aerosol layers and temporal variations concerning the aerosol distribution.

4 Lidar Set-up

One important part of the work behind this thesis has been the development of the lidar equipment. The set-up used in the boundary layer studies, the GÖTE campaigns reported in paper I and II, was located at the roof of the Chemistry department at an altitude around 80 m above sea level (ASL). The laser used was a Nd:YAG laser operated at 532 nm with a repetition rate of 20 Hz. In Fig. 6 a photograph of the vertically directed green laser beam leaving the lidar station booth at the Chemistry department roof.

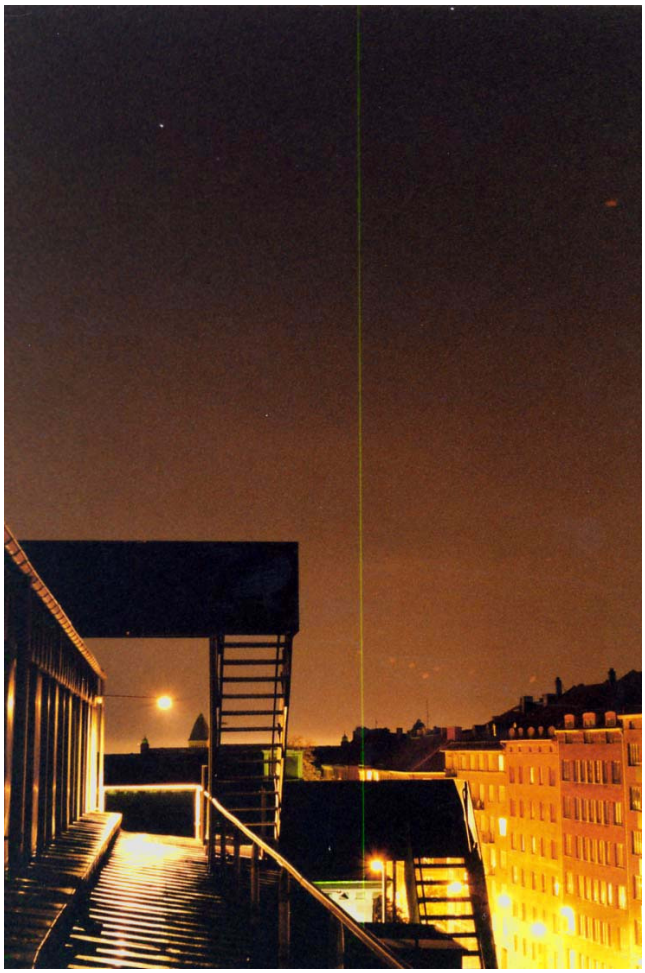

Fig. 6 A photograph showing the vertically directed green laser beam. At the bottom, the beam is exiting the lidar station booth hosting the telescope. The Göteborg city centre is in the background. (photo: Frans Olofson, 2004)

The receiver was a Newtonian telescope with a 30 cm mirror with a focal ratio of 4.1. In the two measurement campaigns focus was on aerosols and their dispersion in the boundary layer, *i.e.* approximately the first km. Consequently, there was a desire to be able to collect light from altitudes as close to ground as possible. During the campaign in paper I the solution to the near-field collection problem was to redirect the laser beam to let it enter the atmosphere coaxially with the telescope. The improved collection efficiency at low altitudes was, however, partly annihilated by PM photon pulse overlap and the range below which data was considered uncertain was found to be around 250 m. Other concerns were directed towards good time resolution and effective filtering of the background radiation during daylight conditions. The background was removed by careful filtering with two interference filters with a half

power bandwidth (HPBW) of 0.5 nm. Since the laser power available was never a problem at these altitudes additional filtering was achieved by means of neutral density filters and compensated for by increased laser output. For the detection of the backscattered light a PM operated in photon counting mode was used. The pulses were counted with a multi channel scaler (MCS) and the height resolution was 15 m. In the work presented in paper II the same lidar set-up was used but with some changes concerning the near field-detection. Instead of a coaxial arrangement the laser beam was emitted parallel to the telescope FOV and a second smaller receiver with a wide FOV was adopted. The use of the second receiver made it possible to accomplish full overlap with the laser beam at only some tens of meters above the telescope. The wide FOV arrangement together with less efficient filtering of course led to a strongly increased background level. However, during a stabile night time period of five hours the two receivers were used in combination and the signals were integrated. This made it possible to shift the wide FOV signal to coincide with the main telescope signal in the range from 0.33 to 1.26 km. Then a ratio between the two signals was calculated and used to extrapolate all main telescope signals from altitudes below 360 m. Thus, it was possible to obtain results down to an altitude of around 60 m. The uncertainty of the ratio however increases at low altitudes as the main telescope signal starts to rapidly fall off.

4.1 The Bistatic Lidar Technique

In paper III and IV the lidar telescope was further developed with the aim to analyze the polarisation properties of the light scattered from ice clouds, *i.e.* cirrus, in a measurement campaign called CABLE (Cooperative ALOMAR Bistatic Lidar Experiment). The measurements were conducted in collaboration with the ALOMAR (Arctic Lidar Observatory for Middle Atmosphere Research) station situated in northern Norway (69° N, 16° E). The principle of the CABLE experiment, illustrated in Fig. 7, was to measure the scattered laser light in a non-backscattering direction, *i.e.* angles other than 180°, so-called bistatic lidar measurements. ALOMAR is situated on a mountain 380 m ASL, while the bistatic telescope was located at a remote site at sea level, a distance of 2.1 km away in the NNE direction. The laser beam was linearly polarised in the E-W direction which gave an azimuth angle, ψ, defined as the angle between the laser polarisation plane and the local scattering plane, of 23.8°. With this geometry the measurements were not restricted to the parallel or perpendicular laser polarisation directions, normally used in depolarisation lidar studies, and in addition a well defined scattering plane was obtained. The concept of CABLE was to simultaneously measure in the backward and off-axis directions by use of the ALOMAR tropospheric lidar transmitter as the primary source. In the measurements the 532 nm wavelength channel has been used, which furnished 290 mJ pulses with 10 ns duration and a repetition rate of 30 Hz. The 532 nm channels of the ALOMAR tropospheric lidar include the parallel and perpendicular polarisation and are given with a range resolution of 7.5 m. The signal was summed for 2000 scans giving a time resolution of about 70 s.

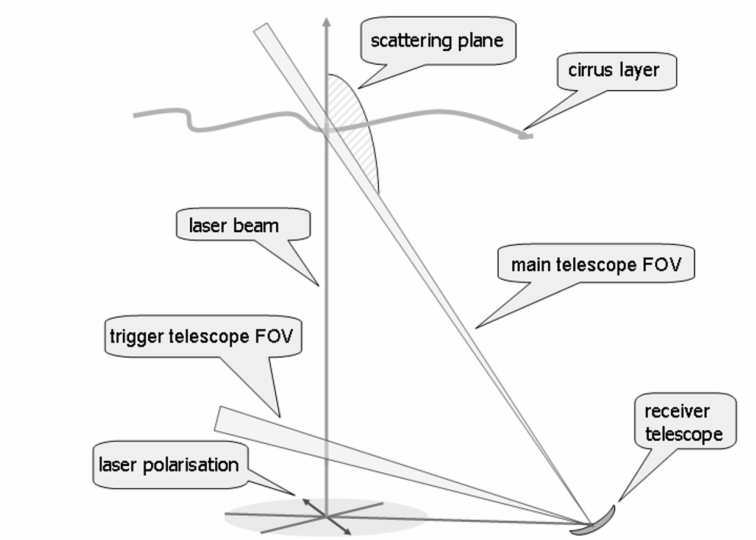

Fig. 7 Schematic view of the CABLE measurement geometry. The remote receiver telescope was located 2.1 km NNE from the lidar station. The laser was polarised in the E-W direction giving an azimuthal angle between the plane of polarisation and scattering plane of 23.8°. The trigger signal was taken from an altitude of roughly 600 m ASL.

To be able to do measurements by looking at the laser beam from aside, the telescope had to be tiltable. This was achieved by mounting it on a photo-theodolite offering careful adjustments in azimuthal and elevation angle. To be able to perform the desired polarisation characterization of the scattered return a polarisation sensitive unit had to be added to the photometer. The polarisation unit consisted of a rotating $\lambda/2$ plate followed by a fixed, vertically aligned dichroic sheet polariser (polaroid). The addition of a rotating $\lambda/2$ plate instead of just a single rotating polaroid has two advantages. First, the period is doubled and second and more important, possible polarisation effects introduced by the optics within the instrument are eliminated. The $\lambda/2$ plate was rotated in 1.8° increments by a stepper motor giving rise to a modulated signal from which the degree of polarisation could be calculated. Since the aim was to do measurements on cirrus a relatively wide telescope FOV of 1° was chosen in order to cover the scattering layer and to make it easier to find it during elevation. The vertical extension of the laser beam and remote telescope FOV overlap is a function of elevation angle, *i.e.* the scattering altitude (Fig. 8). For the filtering of the signal a temperature controlled interference filter was used. The wider FOV related decrease in transmission for such a filter was compensated for by 1 nm HPBW and 2" optics.

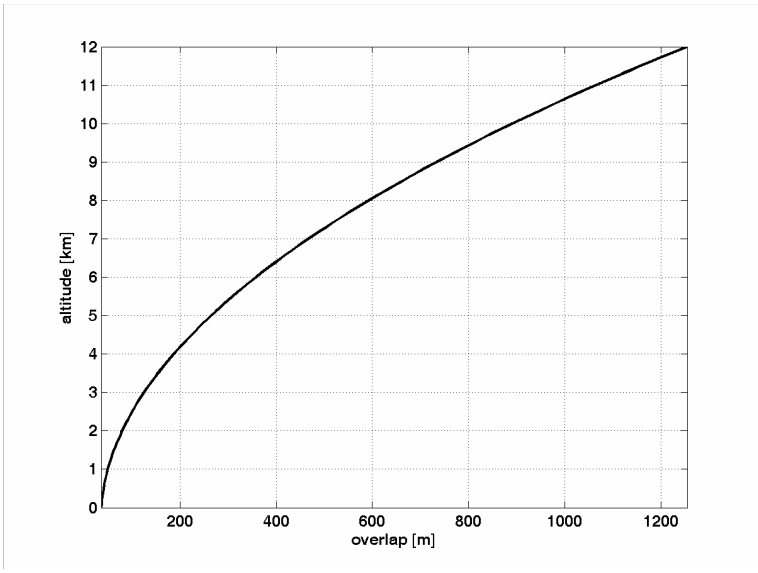

Fig. 8 The vertical extension of the overlap volume as a function of altitude above ALOMAR.

For the accomplishment of the measurements the start of the remote receiver data acquisition had to be synchronised with the laser firing. Because of the separating distance this proved to be a challenge which was further enhanced by the presence of a mountain ridge between ALOMAR and the remote site. Different solutions to the problem, *e.g.* optical fibre and radio communication, was considered and tried. In the end a separate small telescope proved to be sufficient to collect a sync pulse from the laser beam as it became visible behind the mountain, about 230 m above ALOMAR. For the altitudes at which measurements were performed (3 km and above) this arrangement offered more than sufficient time between the arrival of the trigger pulse and the start of the measurement scan. The signal was recorded in the analogue mode on a 300 MHz oscilloscope where it was integrated over 16 or 32 consecutive scans. The choice of analogue recording was required since the signal intensity of scattered light from aerosol layers and clouds can be very high, photon rates exceeding 10^{11} photons/s not being unusual. After each integration the $\lambda/2$ plate was rotated 9° and the profile was stored. The $\lambda/2$ plate polaroid combination yields a modulation of four times the rotation angle, thus a 10-step integration cycle will correspond to a full modulation period. The rotation and storage procedure took some additional time after the integration resulting in a time resolution for the full period of half a min (34 s). The height resolution is dependent on the overlap altitude and length of the measurement scan and ranged from 1 to 7 m. However the effective height resolution was limited by the photomultiplier pulse width to approximately 7 m.

4.2 Data Analysis

The scattered light is encoded by the scattering object and altered in polarisation and/or wavelength. Generally, light is characterised by the electric vector amplitude, $\overline{E}$ whose time dependent part is described by (van de Hulst, 1957)

$$\overline{E}(t,\bar{r}) = \overline{E}_0(\bar{r})e^{i(\omega t+\varepsilon)}, \tag{7}$$

where $\overline{E}_0$ is the electric vector amplitude, $\bar{r}$ is the position vector, ω is the angular frequency, t is the time and ε is the phase. At long distances from a light source the

light wave can be considered a plane wave. If the propagation of the light in the positive z direction is normal to the wavefront and ε is set to zero then the expression for $\overline{E}$ in vacuum is

$$\overline{E}(t,\bar{r}) = \overline{E}_0(\bar{r})e^{i\omega t}e^{-ikz}, \tag{8}$$

where the propagation constant or angular wavenumber $k = 2\pi/\lambda = 2\pi\nu/c$ for a wavelength λ and the speed of light c.

The solution to the wave equation written in spherical coordinates, *i.e.* the spherical wave originating from a point source is

$$\overline{E}(\bar{r}) = \frac{\overline{E}_0(\bar{r})}{ikr}e^{i(kz-kr)} \tag{9}$$

and the amplitude is inversely proportional to the distance, r.

Physical measurements can only sense the longtime root-mean-square average or variance of the amplitude, *i.e.* the radiant energy or intensity. The electric amplitude can be split into two orthogonal polarised components, E_1 and E_2. The two complex amplitudes give rise to four independent and additive combinations of energy parameters. These measurable quantities can be used to fully describe the polarisation state of the light and are called the Stokes parameters. There are three equivalent definitions of the polarisation components (van de Hulst, 1957). These are the polarisation definition,

$$\begin{aligned} I_1 &= \overline{E}_1\overline{E}_1^* \\ I_2 &= \overline{E}_2\overline{E}_2^* \\ U &= \overline{E}_1\overline{E}_2^* + \overline{E}_2\overline{E}_1^* \\ V &= i\left(\overline{E}_1\overline{E}_2^* - \overline{E}_2\overline{E}_1^*\right) \end{aligned} \tag{10}$$

the Stokes definition,

$$\begin{aligned} I &= \overline{E}_1\overline{E}_1^* + \overline{E}_2\overline{E}_2^* \\ Q &= \overline{E}_1\overline{E}_1^* - \overline{E}_2\overline{E}_2^* \\ U &= \overline{E}_1\overline{E}_2^* + \overline{E}_2\overline{E}_1^* \\ V &= i\left(\overline{E}_1\overline{E}_2^* - \overline{E}_2\overline{E}_1^*\right) \end{aligned} \tag{11}$$

and the circular definition,

$$\begin{aligned} I &= a^2 \\ Q &= a^2\cos 2\beta\cos 2\chi \\ U &= a^2\cos 2\beta\sin 2\chi \\ V &= a^2\sin 2\beta \end{aligned} \quad . \tag{12}$$

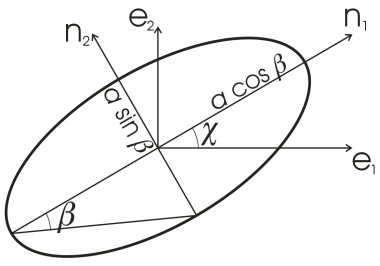

Fig. 9 The polarisation ellipse defining the state of polarisation for arbitrary polarised light. β describes the ellipticity and χ gives the orientation of the polarisation.

The circular definition is a geometric representation, which in an illustrative way describes the polarisation concept by the ellipticity (ratio of the long and short axis) and orientation of the so-called polarisation ellipse, shown in Fig. 9. A plane of reference is chosen which is spanned by the direction of propagation and the unit vector $\mathbf{e}_1$. The unit vector $\mathbf{e}_2$ is normal to the reference plane. The unit vectors $\mathbf{n}_1$ and $\mathbf{n}_2$ are oriented along the long and short axes respectively of the ellipse. Consider a beam of light travelling into the paper along the normal, then the ellipse is the trace of the tip of the electric field vector, for the general case of elliptically polarised light. The ellipticity is given by $\tan\beta$ and is 0 for linearly polarised light, and -1 and +1 for left-handed and right-handed circularly polarised light, respectively. The orientation of the ellipse is given by χ (van de Hulst, 1957). Another way to define the Stokes parameters is as the total intensity (I), the excess of perpendicular polarised light over parallel polarised light (Q), the excess of +45° oriented polarised light over -45° oriented polarised light (U) and the amount of circularly polarised light (V). The definition is valid for a vertical reference plane and for positive rotation being clockwise.

The interaction of light with matter can be regarded as a linear transformation of the orthogonal amplitudes, E_1 and E_2. The transformation is represented by a Jones amplitude matrix, $\tilde{S}$ defined by the properties of the medium. The intensity of the scattered light, I_{scatt} becomes,

$$I_{scatt} = \overline{E}_{scatt}\overline{E}^{*}_{scatt} = \left(\tilde{S}\overline{E}_{inc}\right)\left(\tilde{S}\overline{E}_{inc}\right)^{*} = \overline{E}_{inc}\left(\tilde{S}\tilde{S}^{*}\right)\overline{E}^{*}_{inc}, \tag{13}$$

where the subscript *inc* refers to incident. Since the physically measurable quantity is the intensity it is in practice more convenient to define a 4×4 transformation matrix, the Müller scattering matrix, for the calculation of the Stokes parameters of the scattered light

$$\begin{bmatrix} I \\ Q \\ U \\ V \end{bmatrix}_{scatt} = \frac{1}{k^2 r^2}\begin{bmatrix} m_{11} & m_{12} & m_{13} & m_{14} \\ m_{21} & m_{22} & m_{23} & m_{24} \\ m_{31} & m_{32} & m_{33} & m_{34} \\ m_{41} & m_{42} & m_{43} & m_{44} \end{bmatrix}\begin{bmatrix} I \\ Q \\ U \\ V \end{bmatrix}_{inc}. \tag{14}$$

The elements of the Müller matrix are functions of scattering angle and the physical properties of the scattering objects, *i.e.* for particles, the size, shape and chemical composition. Depending on symmetry properties of the scattering media part of the matrix elements vanish and the Müller matrix is reduced. For an ensemble of particles which are randomly oriented and contain a plane of symmetry the matrix becomes (van de Hulst, 1957)

$$\begin{bmatrix} I \\ Q \\ U \\ V \end{bmatrix}_{scatt} = \frac{1}{k^2 r^2}\begin{bmatrix} m_{11} & m_{12} & 0 & 0 \\ m_{12} & m_{22} & 0 & 0 \\ 0 & 0 & m_{33} & m_{34} \\ 0 & 0 & -m_{34} & m_{44} \end{bmatrix}\begin{bmatrix} I \\ Q \\ U \\ V \end{bmatrix}_{inc}. \tag{15}$$

The above scattering matrix provides a very good description of the scattering properties of many types of collections of randomly oriented aerosol particles, *e.g.* a

cloud, and is by far the most used in calculations (Mishchenko *et al.*, 2005). The light from the sun is randomly polarised, for which the Stokes vector is $[1\ 0\ 0\ 0]^T$. In the case of lidar studies the laser is normally linearly polarised, vertically or horizontally. The Stokes vector of the light incident on the scattering volume is $[1\ \pm1\ 0\ 0]^T$ but the laser can also be circularly polarised with the corresponding vector, $[1\ 0\ 0\ \pm1]^T$.

In the CABLE geometry the laser Stokes vector had to be transferred to the scattering plane coordinate system, which yields $[1\ \cos2\psi\ \sin2\psi\ 0]^T$. ψ is the azimuthal angle between the laser polarisation plane and the scattering plane, which during the CABLE campaign was 23.8°. Depending on which physical property is the one of interest a range of assumptions has to be made to derive the elements of the Müller matrix. Concerning the composition, the refractive index of water or ice can be used if it is tropospheric clouds that are studied. There are many so-called type aerosols with tabulated refractive indices, *e.g.* the AERONET sun photometer program (summarized in Omar *et al.*, 2003). When more than one wavelength is introduced in light scattering experiments information about particle size is gained. Size distributions are often considered of log-normal type. This is true for an aged aerosol which has had time to undergo coagulation and condensation. However, in other cases like dust plumes or clouds this is probably not true and *e.g.* Gaussian or exponential distributions can be used. If the particles are not spherical the scattered light will be depolarised. This is utilised for characterization of particle shape, *e.g.* in cirrus. Non-spherical particles primarily affect polarisation conditions at scattering angles between 100° and 170° (Ward *et al.*, 1973; Liou and Takano, 2002; Mishchenko and Sassen, 1998).This normally requires a bistatic technique using a receiver physically displaced from the laser transmitter. Orientation of large ice crystals in cirrus gives rise to specular reflection as shown in measurements by Borovoi *et al.* (2008).

Exactly one century ago the Lorenz-Mie formulae were first published and have since then been used to predict scattering from objects approximated by spheres. For larger spheres and non-spherical particles where the analytical form of the Mie formulas become unpractical ray tracing and geometric optics have been used (van de Hulst, 1957). In the past few years computer codes have been developed for scattering by non-spherical, rotationally symmetric particles. Mishchenko has exploited the *T*-matrix method, originally developed for acoustics by Waterman (1969) and later applied to the electromagnetic case (Waterman, 1971). With the *T*-matrix method the scattering properties are separated into one part only dependent on the physical properties of the particles and one part dependent on the orientation of the particle with respect to the incident light. The elements of the *T*-matrix are expanded in generalized spherical functions, equivalent to the Wigner polynomials known from angular momentum theory. Since for a given case, *i.e.* scattering angle, the matrix elements are only functions of shape, size and composition of the particles the computation time is substantially reduced. The method is, however, restricted to moderate aspect ratios and fairly small particles (Mishchenko & Travis, 1998). An alternative method for calculation of scattering by non-spherical particles of in principle any shape is the discrete-dipole approximation (DDA). In this method the particle is thought of as consisting of a lattice of radiating dipoles. The resulting electrical field is calculated from the corresponding linear equations and then converted into the resulting scattering matrix (Purcell & Pennypacker, 1973). Other methods used to solve the non-spherical particle scattering problem that can be mentioned are the finite-difference time domain (FDTD) (Taflove, 1995) method and a long range of modifications of the Lorenz-Mie formulas, (*e.g.* van de Hulst, 1957).

The objective with the measurements was to perform a polarisation analysis of the scattered laser light. The polarisation analyser of the remote receiver consisted of a rotating $\lambda/2$ plate followed by a fixed polaroid. This combination gives rise to a modulated signal from which it is possible to calculate the degree of polarisation. The peaks in the modulation arise when the polarisation analyser maximum transmission axis and the plane of highest linear polarisation of the scattered light coincides. Conversely, when they are perpendicular a modulation valley is instead the result. Figure 10 shows results from a measurement on October 19th, 2006 during cloud free conditions in the altitude region between 6.1 and 6.4 km.

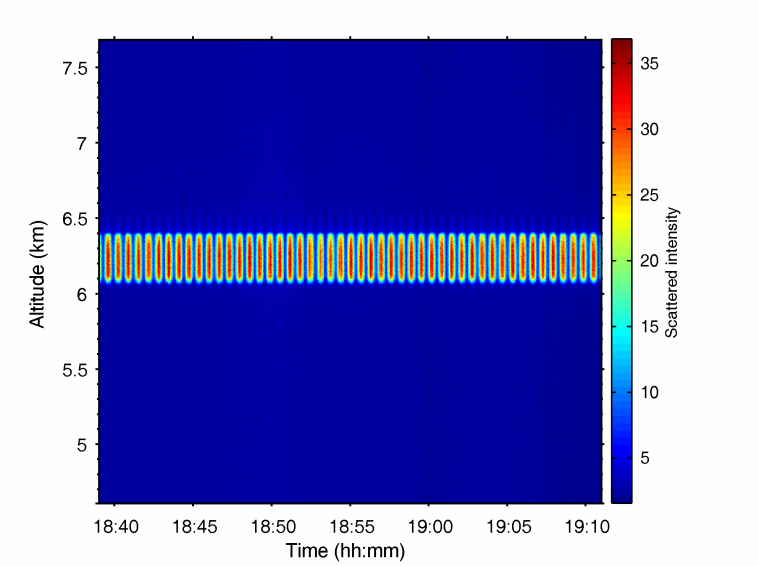

Fig. 10 Colour panel showing the modulated signal from a cloud free overlap region between 6.1 and 6.4 km. The background signal is recorded in the blue area before and after the overlap region. Signal strength is given in arbitrary units.

The modulated stripe in the middle is the actual signal of the scattered laser light. The altitude region responsible for the signal is the region where the telescope FOV intercepts the laser beam, hereafter called the *overlap region* (recall Fig. 7). The blue areas correspond to times in the measurement scan before and after the overlap region interception of the laser pulses, *i.e.* the blue area is the background signal. After the background has been removed the signal is altitude averaged in the overlap region. The intensity extremes in the modulated signal are referred to as $I_{\max}$ and $I_{\min}$, respectively and the degree of linear polarisation, P_{L} is calculated from,

$$P_L = \frac{I_{\max} - I_{\min}}{I_{\max} + I_{\min}}. \qquad (16)$$

The polarisation properties of the scattered light is contained by the four Stokes parameters. Figure 11 illustrates the function of the polarisation analyser showing the modulation for each of the four Stokes parameters as function of the $\lambda/2$ plate rotation angle.

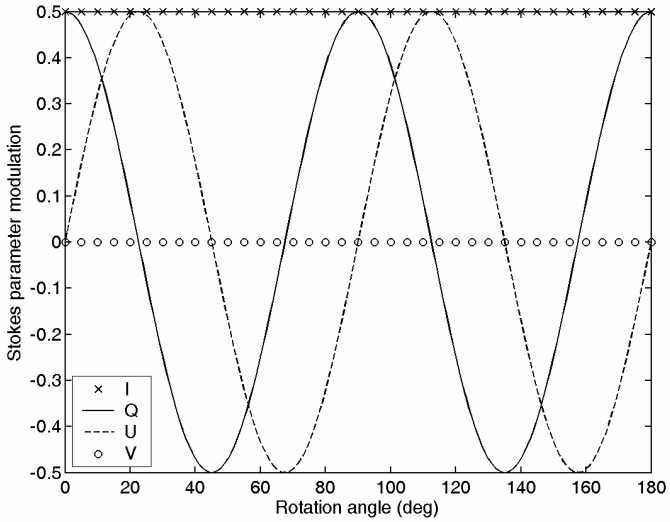

Fig. 11 Modulation of the four Stokes parameters of the transmitted light by a rotating $\lambda/2$ plate – fixed polaroid combination (I: crosses, Q: solid line, U: dashed line & V: circles).

The polarisation analyser transformation of the light can be described by multiplication of the scattered incoming light Stokes vector (*scatt*) with the general transformation matrix of the retardation plate (*ret*) and the transformation matrix of the vertically aligned polaroid (*pol*), (Bohren & Huffman, 1998). The Stokes vector of the transmitted light (*trans*) is then expressed as,

$$\begin{bmatrix} I \\ Q \\ U \\ V \end{bmatrix}_{trans} = \tfrac{1}{2}\begin{bmatrix} 1 & 1 & 0 & 0 \\ 1 & 1 & 0 & 0 \\ 0 & 0 & 0 & 0 \\ 0 & 0 & 0 & 0 \end{bmatrix}_{pol} \begin{bmatrix} 1 & 0 & 0 & 0 \\ 0 & C^2+S^2\cos\delta & SC(1-\cos\delta) & -S\sin\delta \\ 0 & SC(1-\cos\delta) & S^2+C^2\cos\delta & C\sin\delta \\ 0 & S\sin\delta & -C\sin\delta & \cos\delta \end{bmatrix}_{ret} \begin{bmatrix} I \\ Q \\ U \\ V \end{bmatrix}_{scatt} \quad (17)$$

where $C = \cos 2\varphi$, $S = \sin 2\varphi$, and δ is the retardance, *i.e.* the resulting phase shift between the components along the fast and slow retarder axis. φ is the angle of rotation from the zero position, *i.e.* the local vertical. For a $\lambda/2$ plate $\delta = 180°$ which together with some trigonometry results in the expression for the total intensity of the light detected by the PM,

$$I_{trans} = \tfrac{1}{2}\left(I_{scatt} + Q_{scatt}\cos 4\varphi + U_{scatt}\sin 4\varphi\right). \quad (18)$$

From the definition of the Stokes parameters (van de Hulst, 1957) it follows that the total degree of polarisation of a monochromatic light wave is,

$$P = \frac{\sqrt{Q^2+U^2+V^2}}{I} \le 1. \quad (19)$$

For a single polarised light beam the light scattered from a system of identical particles this parameter is constant and equals unity independently of the scattering angle. For non-identical particles the expression is always less than unity, a consequence of polydispersity. As an example, the scattering by randomly oriented molecules with anisotropic polarisability can be regarded as the sum of a Rayleigh scattering component and an angularly isotropic component (van de Hulst, 1957) and

consequently $P < 1$ at all scattering angles. The fixed polaroid, rotating $\lambda/2$ plate combination used in the measurements presented in this thesis allowed the Stokes parameters I, Q and U to be determined from a set of a minimum of three independent angular measurements. The received intensity was measured at ten separate angular settings, which gave rise to an over-determined system of equations that was solved by standard matrix inversion technique. From I, Q and U another expression for the polarisation can be constructed,

$$P_L = \frac{\sqrt{Q^2 + U^2}}{I}, \tag{20}$$

which is called the degree of linear polarisation (Bohren and Huffman, 1998; Mishchenko *et al.*, 2005). This parameter is exactly the same as the one retrieved from the experimental data, by Eq. 16, and has been used to analyse the bistatic lidar measurements.

4.3 Alternative Measurement Approaches

Lidar studies are often carried out together with other types of measurements. The techniques that will be presented here can also be used as complements or be combined among themselves. The purpose is to collect as much information as possible and the extent of the research study is as always a question of access to instrumentation and economic resources.

4.3.1 Sun Photometer

The concept of sun photometers is to measure the direct sun light and calculate the attenuation (Holben *et al.* 1998). For this the Beer–Lambert–Bouguer's law is used, which relates the intensity of the light at top of the atmosphere (TOA) to that measured at ground. To retrieve the TOA intensity a so-called Langley plot is constructed, in which the measured intensity is plotted as a function of solar zenith angle. By extrapolating the curve to zero atmospheric thickness the TOA intensity is retrieved and can be used to calculate the optical depth (optical thickness) of the atmosphere. The sun light attenuation can be divided into three contributions, molecular and aerosol scattering and absorption, mainly by ozone. The molecular scattering and ozone absorption is derived from model atmospheres. Left is the aerosol contribution which is expressed as the aerosol optical thickness (AOT). The AOT is dependent on the wavelength which was established by Ångström (1929). If the AOT is measured at two different wavelengths the spectral dependence may be approximated as a power law relationship between the corresponding ratios of AOTs and wavelengths. The exponent is called the Ångström exponent, α and is small for large particles and vice versa. Furthermore α can be related to the size distribution. Today sun photometer measurements are conducted on routine basis around the world, *e.g.* the AERONET program (Holben *et al.* 1998). A variation of the sun photometer concept uses the near forward scattered sun light, the *aureole*, to extract more information. Avoiding the direct sun light, measurements are performed to determine the phase function at scattering angles up to typically 10 – 15°. Such measurements can be used to derive size distributions and refractive index (Twitty, 1974).

4.3.2 *In situ* Measurements

Direct sampling of aerosols and cloud particles is a very good way to get reliable information on the studied particles. On the other hand it is difficult to cover large areas and to know how representative the measurements are on a larger scale and it also involves being at place, which demands for airplanes or balloons. The instruments carried onboard are much the same as those used at ground, *e.g.* size segregation instruments like, impactors, cyclones and scanning mobility particle sizers, instrumentation for chemical characterization like, filters and aerosol mass spectrometers and black carbon absorption instruments *etc*. Of particular interest in this thesis are cirrus clouds. Among the different studies the ones performed by Heymsfield *et al.* (1990) can be mentioned. They used airborne optical imaging probes and high-resolution microphotography to determine size distributions. Also the ice water content (IWC) was measured.

4.3.3 Spaceborne Measurements

Nowadays, there are numerous satellite sensors with optical or spectroscopic aerosol detection capability. The MODIS satellite measures radiation in a broad spectral range (0.4 - 14.4 μm) to obtain information about the AOT, the Ångström exponent and aerosol type (http://modis-atmos.gsfc.nasa.gov/index.html). The CALIPSO satellite uses a dual wavelength lidar (1064 & 532 nm) with cross polarisation utility (532 nm) for vertical profiles of aerosols and thin clouds (*e.g.* optical depth, backscatter and extinction coefficient) and a thermal infrared radiometer (8.7, 10.5 mm & 12.0 mm) to obtain information about temperature and particle size for cirrus (http://www-calipso.larc.nasa.gov/). Satellite observations provide global data on atmospheric properties and are excellent for large scale and climatological studies. For local studies the spatial resolution may still be too low.

4.3.4 Radar

Radar uses the same principle as lidar but instead of light radiation of much longer wavelength is used, typically microwaves to radio waves. The technique was originally used to detect large distant objects, like military ships during World War II. The radar technique is also very suitable in a meteorological context for detection of precipitation. According to electromagnetic scattering theory the magnitude of the scattering depends and increases with size and hence, the long wavelength of microwaves and radio waves makes it difficult to detect small sub-micrometre aerosol particles. However, during the last decade development of the high spectral resolution Doppler radar technique has made it possible to detect cirrus and retrieve microphysical properties, *e.g.* size and IWC (Matrosov, 1997; Mace *et al.*, 2002).

5 Results from the Lidar Measurement Campaigns

In this section the results from the measurement campaigns conducted in Göteborg and Northern Norway are presented. Papers I and II of this thesis describes investigations performed during the GÖTE campaigns in 2004 and 2005. In paper III and IV the scattering properties of high latitude aerosols and clouds, with emphasis on cirrus, were investigated with a bistatic lidar technique in the CABLE campaign.

5.1 Urban Aerosol Development Connected to Temperature Inversion

The campaigns were a joint effort from several groups in the Göteborg region with the overall aim to study the air quality in, and around, the city and to better understand the effects of boundary layer dynamics. The research interests concerned monitoring of particulate and gaseous pollutants during episodes of temperature inversion for characterisation of dispersion patterns and size segregation and chemical speciation of particles. The results were also implemented in an air pollution model. The measurements reported in this thesis concern the effects of winter temperature inversion episodes on the pollutant levels and the aerosol dispersion trends. During nights with clear sky and low wind speeds effective radiative cooling of the ground together with lack of turbulence may give rise to a temperature inversion. The limited mixing in the ground inversion layer in combination with morning rush hour emissions can heavily reduce the urban air quality. The drastically increased particle concentration often experienced during inversion episodes is known to constitute a threat to human health (Dockery *et al.*, 1993; Pope *et al.*, 1995; Pope *et al.*, 2002). The morning particulate emissions in Göteborg are greatly influenced by traffic. In the studies emphasis was put on aerosols which were monitored by the lidar and with ground-based and airborne SMPS systems. To further aid in the interpretation of the aerosol data, meteorological data and measurements of traffic related trace gases such as CO, NO and NO_2 were also used. The lidar data are presented as range corrected signal and the time as local time (UTC+1).

When the inversion layer breaks up in the morning the pollutants trapped during the night are released and dispersed into the residual layer of the boundary layer. The rate of the mixing depends on energy available from the insolation, which heats the ground and offers conditions of increased wind speed.

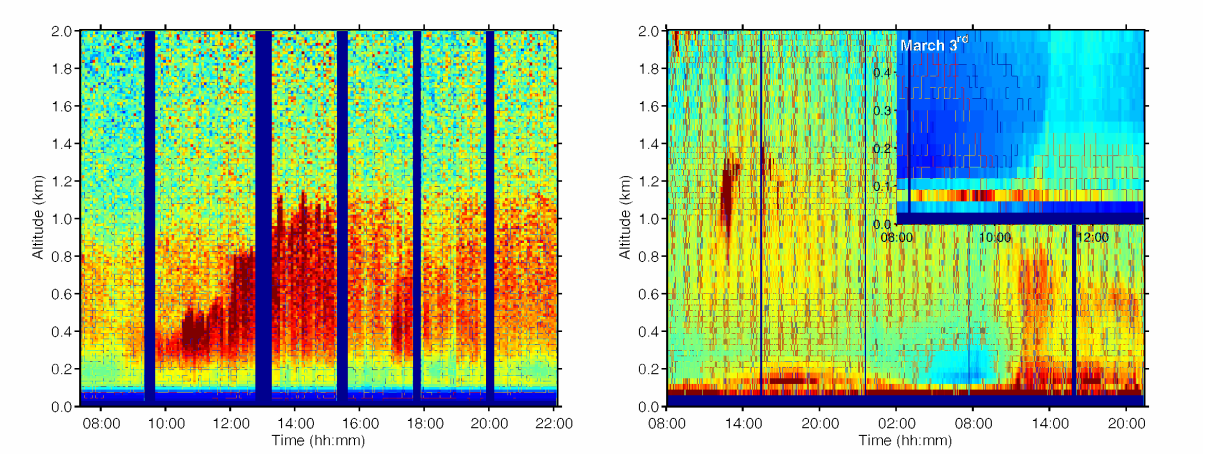

Fig. 12 Range corrected lidar signal from 07:20 – 22:05, March 4th 2004 (left panel) and from 08:00, March 2nd – 21:24, March 3rd 2005 (right panel). The inset in the right panel shows the details in the morning and around noon on March 3rd, 2005

The longer the pollutants are confined to the surface layer the more they exert negative effects on health. The mixing rate can therefore be of concern. In Fig. 12 two examples are shown in which an inversion layer break-up was followed. To the left is a measurement from March 4th 2004 and to the right a measurement from March 2nd to March 3rd 2005. The latter example shows both a morning characterised by a relatively well mixed boundary layer (March 2nd) and a morning following a night with an inversion layer (March 3rd). The two inversion layer break-up episodes are quite different. In the left case the start of the mixing onset agreed well with the sunrise, around 07:30, and the increased scattering from the rising particulate pollutants resulted in a mixing rate of around 200 m/h. In the right case on the other hand it took until around 10:00 before sufficient heating of the ground broke up the inversion layer. The details are shown in the figure inset. Once started, the convective mixing became rapid and resulted in a mixing rate close to 800 m/h during one hour.

During periods without a wintertime temperature inversion mixing may still not be very efficient due to the limited insolation at high latitudes. This was demonstrated in the afternoon on March 2nd, 2005 by the inefficient dispersion of rush hour pollutants giving rise to increased scattering up to about 250 m. The two examples are however from the same part of the year and the insolation was about the same. One explanation to the later inversion break-up onset in the 2005 example above can be found in the temperature. The temperature during the night between 2nd and 3rd of March, 2005 was much lower than the corresponding night the year before which required an extended heating of the ground and surface layer. Since the lidar was placed at 80 m ASL and because of the poor light scattering collection at low altitudes the actual time for the break-up could not be directly followed. However, if the trends of particulate mixing are extrapolated down to ground level the onset of inversion layer break-up could be established to typically one to three hours after sunrise.

5.1.1 Results from Additional Measurement Techniques

During the GÖTE campaigns several techniques other than lidar were used. In the 2005 campaign reported in paper II, airborne particle measurements were carried out. Onboard a small four-seated aircraft two different aerosol instruments were installed, one ultrafine particle counter (P-TRAK) and one scanning mobility particle sizer (SMPS). The P-TRAK measured the total number concentration for particles between 20 nm and 1 µm, and the SMPS measured particle size distributions between 10 and 300 nm.

Airborne *in situ* measurements makes it possible to obtain absolute numbers for particle concentrations and size distributions, while that is a difficult task for the lidar. Furthermore the airborne measurements can be used to study the horizontal movement of the aerosol. However, the use of an airplane is expensive, and can be used for comparisons on selected days.

In Fig. 13 an example of a P-TRAK measurement (solid line) from March 9th, 2005 is shown. The dashed curve shows the average lidar profile from the same time period. From the lidar measurement reduced mixing was observed up to around 400 m, suggesting an inversion layer. In the residual layer the backscattering was nearly constant up to around 1200 m, where the signal started to increase again. The explanation may be increased scattering from condensation activated particles. The P-TRAK measurement shows a rapid decrease in concentration to 100-200 particles/cm^3 below the cloud base at around 1600 m revealing the transition to the free troposphere. Within the residual layer between 300 and 1600 m, the particle concentration decreased gradually from around 2000 particles/cm^3. The fluctuations reflect local horizontal differences and temporal variations not accounted for in the lidar measurement.

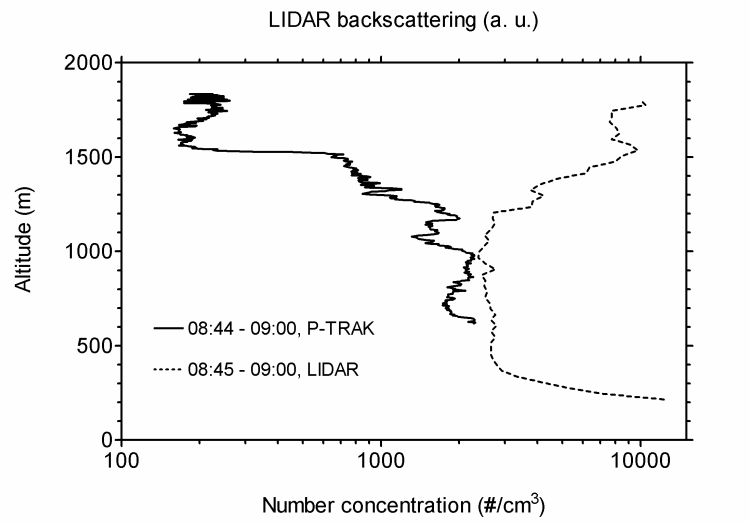

Fig. 13 Vertical profiles of total number concentration (0.02 – 1 µm) (solid line) and lidar backscattering (a. u.) (dashed line) in the morning on March 9th 2005.

The explanation for elevated number concentrations can be found in the SMPS measurements. In Fig. 14 size distributions from 580, 1080 and 1810 m ASL measured between 08:01 and 09:01 are shown. At 1810 m, representing the free troposphere, an accumulation mode peaking around 400 particles/cm^3 was found but the size distributions at 580 and 1080 m also revealed elevated levels of nuclei mode particles throughout the boundary layer. The accumulation mode is characteristic of an aged aerosol, while the nuclei mode particles indicate newly formed or emitted particles (Hinds, 1999).

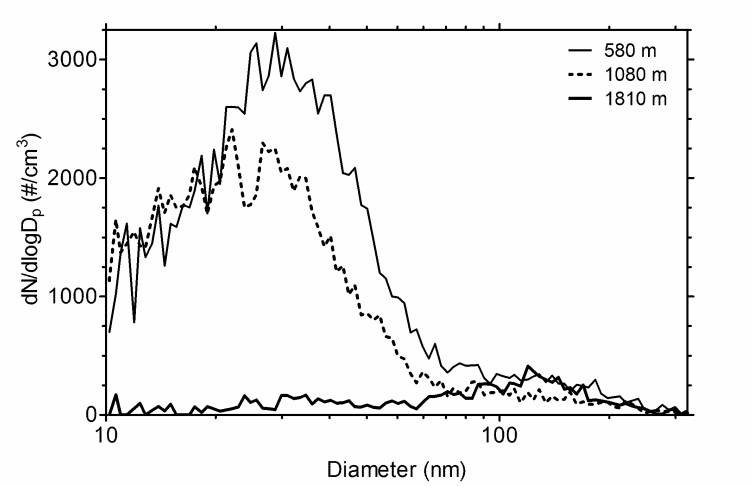

Fig. 14 Airborne SMPS measurements above Göteborg 08:01 – 09:01, March 9th at three different altitudes; 580 m (thin solid line), 1080 m (dashed line) and 1810 m (thick solid line).

The nuclei mode particles, occurring in high concentration, at the lower altitudes in Fig. 14 showed size distributions peaks around 20 to 30 nm. Such distributions are typical for those obtained from petrol road traffic emissions (Wehner *et al.*, 2002; Molnár *et al.*, 2002; Janhäll *et al.*, 2004, Janhäll & Hallquist, 2005) and an up-transport during the boundary layer mixing the day before could be expected. On the other hand, one might expect particle growth during the night. This indicates that nucleation may have taken place in the residual layer during the night and early morning. Production of new aerosols throughout the boundary layer has recently been reported by Boy *et al.* (2004).

The size distribution evolution during March 2nd, 2005, shown in Fig. 15, revealed another indication of a particle nucleation event. At around 14:00 the development of what appeared to be a so-called nucleation banana started, *i.e.* an increase in concentrations at the smallest diameters together with an apparent growth of the particles. The event was preceded by an hour of relatively clean air limiting the total surface area available for condensation and coagulation. This made the probability for low volatile compounds present to condense and nucleate higher. Hence, the small initial particle sizes that grew with time, the appearance of these particles during a time period with relatively low activity during the day, and the fact that the event was preceded by a short period with relatively clean conditions suggest that nucleation of new particles took place. Nucleation was further governed by low temperature, staying below -3 °C. The growth rate of newly formed particles in the size range from 10 to 30 nm was estimated to 3.5 ± 1 nm/h, which is within the range from 2 to 10 nm/h previously observed in urban environments (Kulmala et al., 2004; Holmes, 2007).

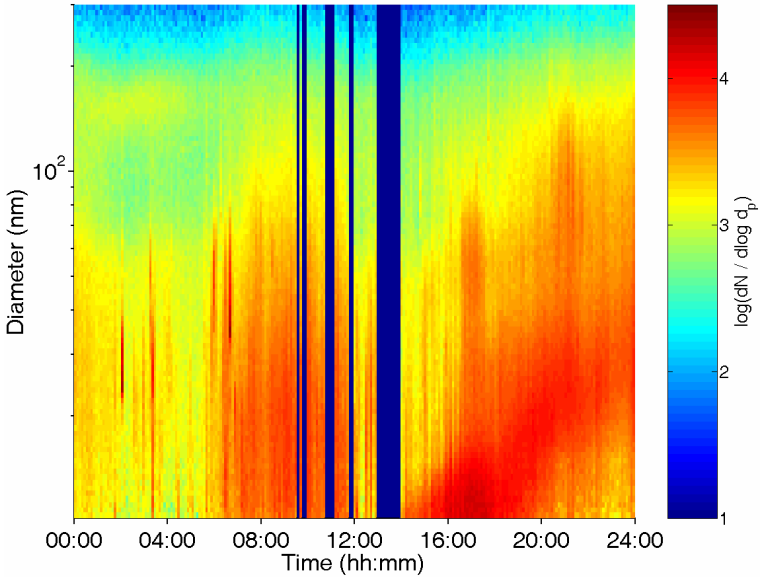

Fig. 15 Particle size distributions during the period March 2nd, 2005. The particle concentration (dN / dlog d_p) is represented on a logarithmic scale.

The airborne particle measurements performed on March9th, 2005 were not confined only to regions above the city centre, but also included measurements along the coast line. The wind direction that day was ENE at low altitudes with a shift to a prevailing NNE direction higher up, which thus made it possible to study the city plume. Since the particle concentrations in the plume can be considerably higher compared to suburban or rural background levels the movement and aerosol development is of importance to air quality and atmospheric processes.

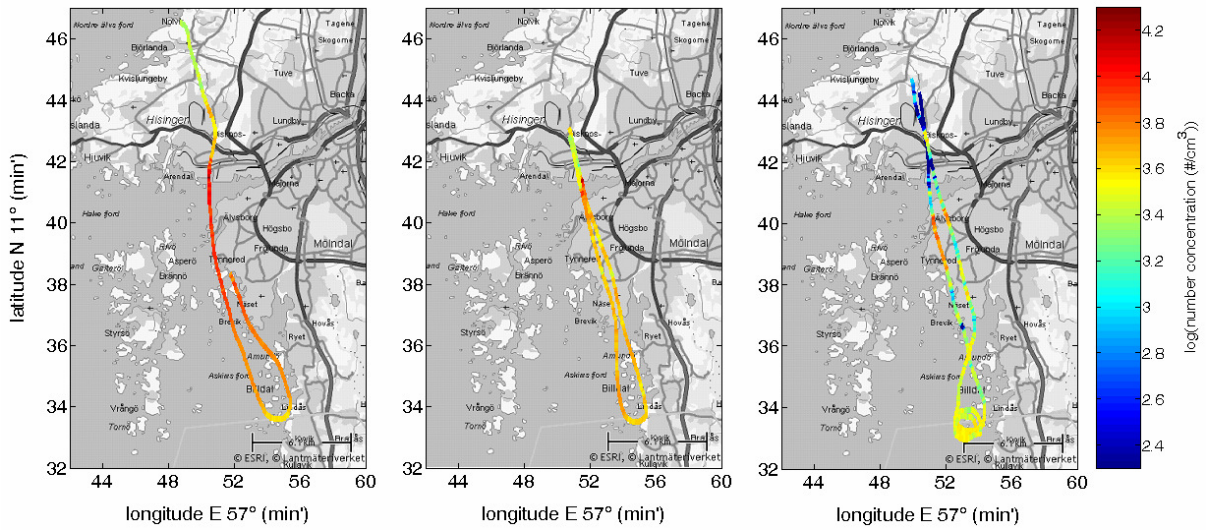

Fig. 16 Airborne measurements of total particle number concentrations (0.02-1 µm) on March 9th, 11:22 – 12:05 along the coast west of Gothenburg at three different altitudes: 183 m (left panel), 426 m (middle panel) and 1077 m (right panel). The particle concentration (particles/cm^3) is represented on a logarithmic scale.

Figure 16 shows number concentration measurements along the coast line at three different mean altitudes (183 m 426 m and 1077 m) between 11:22 and 12:05, March 9th, 2005. In the maps of the coast line the flight paths are shown in colour code, ranging from blue to red with increasing particle concentration. The Göteborg harbour located at the outlet of the river Göta älv running through the city is the biggest in the Nordic region, and a large proportion of Sweden's international trade

passes through here. The city plume transported by the wind along the river canyon was detected as a smooth particle concentration increase. With increasing altitude the plume moved southwards. The city plume was broken by sudden spikes thought to originate from local harbour sources. In particular one spike was persistent and therefore not likely caused by shipping, but instead interpreted as a stationary source on the northern bank of the river. Over areas north and south of the harbour the appearance of these spikes were less frequent.

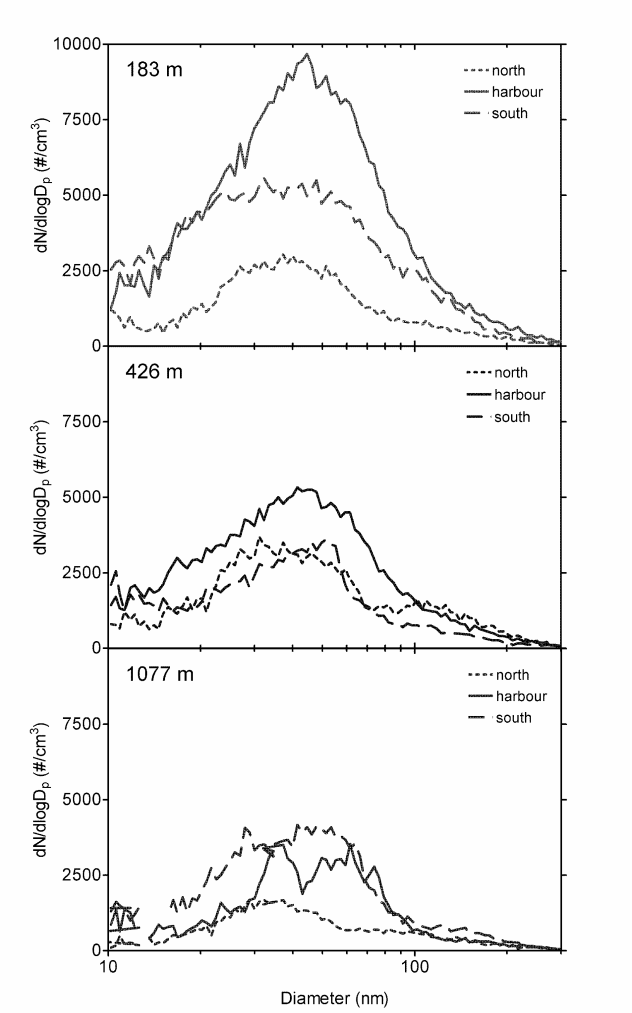

Fig. 17 Airborne measurements of particle number size distributions on March 9th, 2005. Measurements were performed along the coast at three different altitudes; 183 m, 426 m and 1077 m. The solid lines represent distributions measured above the harbour area. Measurements north and south of the outlet are displayed with the dashed and dotted lines, respectively.

The city plume was further characterised by number size distribution measurements from the flight paths shown in Fig. 16. (These are results that have not been reported in paper I or II.) Figure 17 shows the distributions, divided according to airplane position with respect to the harbour, north, above and south. As expected, the concentrations decreased with altitude and were generally lowest north of the harbour. The movement of the plume southwards with increasing altitude is realized if the harbour and south concentration are studied. At 183 m the south concentration is roughly half of the harbour concentration, while at 1077 m the south concentration is the highest of the three. At all three altitudes the majority of the particles were in a mode peaking around 40 nm, while the accumulation mode particles made a minor contribution. The size distributions in Fig. 14 peaked around 20 – 30 nm and traffic emissions are known to have similar distributions. This implies that the particles in the city plume had increased in size with approximately 15 nm during the three hours from 9 am to noon.

The boundary layer dynamics are concluded to have a strong impact on the properties of the urban aerosol and to a large extent determine the severity of the wintertime urban air pollution episodes. The limited insolation in wintertime sometimes resulted in near neutral boundary layer conditions, and the polluted layer near ground was often inefficiently ventilated during the day. In the case of temperature inversion episodes the break-up was observed during the time period 08:00 – 14:00. The mixing process was, however, sensitive to the detailed meteorological conditions and the rate of rising of polluted air within the residual layer varied considerably. Rates between 200 and 800 m h^{-1} was observed. Also the onset of inversion layer break-up varied from around 08:00 – 10:00. Recently formed particles were observed around midday subsequent to surface layer ventilation. High concentrations of nuclei mode particles

observed during airborne measurements in the residual layer also suggested that nucleation may take place at higher altitudes within the boundary layer.

5.2 Polarisation Characterisation of Arctic Tropospheric Aerosols and Clouds

Cirrus clouds are known to consistently cover 20 – 30 % of the Earth's surface (Liou *et al.*, 1986; Wylie *et al.*, 1994). The microphysical properties, *e.g.* size, type of size distribution and shape, of the cloud particles influence how electromagnetic radiation is scattered through the cloud. Cirrus are ice clouds and hence the particles are non-spherical. Scattering by non-spherical particles alters the polarisation state of the light. This fact is widely used to distinguish non-spherical particles from spherical by means of lidars with channels for the parallel and perpendicular polarisation components of the scattered return. In the CABLE measurements the scattered laser light was collected by a remote polarimetric receiver. Conventional backscatter lidars have an infinite of equivalent scattering planes in the 180° backscattering direction but with the bistatic geometry the degeneracy is eliminated. The choice of a non 180° scattering angle also eliminates the zero depolarisation of specular reflection from horizontally oriented ice particles being misinterpreted as scattering from spherical particles. The measurements were performed at altitudes in the range 1.5 – 11 km corresponding to 130 – 170° which are scattering angles known to be sensitive to particle shape (Ward *et al.*, 1973; Mishchenko & Sassen, 1998; Liou & Takano, 2002). The aim of the CABLE campaign was to extend the scientific output from a lidar system with the ultimate purpose of improved understanding of the radiative properties of layered clouds. The off-axis profiles are presented as the raw data signal and the backscattering profiles as range corrected signal and the time as UTC (LT-2).

To interpret the degree of linear polarisation obtained from the experiments calculations using Lorenz-Mie theory for spherical particles (van de Hulst, 1957) and the *T*-matrix approach for non-spherical, rotationally symmetric particles (Mishchenko *et al.*, 2005) were performed. The calculations have been performed for 532 nm and for the scattering angles from 130 to 170°. The aerosol particles or the particles in a cloud are not monodisperse but have a size distribution and this had to be accounted for in the calculations. For spheres the scattering from 5000 individual randomly generated sizes within the specified distribution was summed. For the *T*-matrix code routines for integration of the scattered light over the particle size distributions were used. Due to limitations of the *T*-matrix method the sizes and aspect ratios had to be kept moderate. In the calculations the radius was generally around 1 μm and the aspect ratio in the range 1/2 – 2. The calculations are especially demanding for prolates (Mishchenko *et al.*, 1998).

5.2.1 Bistatic Lidar Measurements

The idea of the CABLE campaign was to extend the range of information obtained from an ordinary lidar by complementary measurements with a bistatic system. In Fig. 18 results from the period 18:52 – 19:20 on October 20th, 2006 is shown. The left panel shows the off-axis measurement and the right panel the corresponding altitude interval for the backscattering measurement. The overlap region, the altitude interval where the remote receiver FOV and the laser beam overlap, extended from 7.45 to 7.85 km.

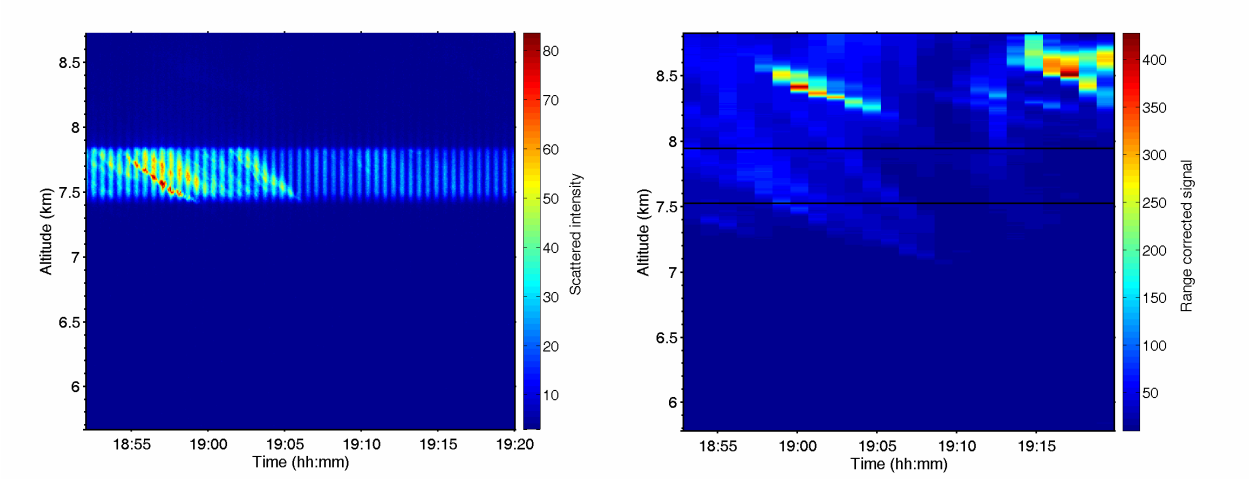

Fig. 18 A comparison between the off-axis measurement from the remote site (left panel) and the backscatter measurement from the lidar station (right panel). The horizontal lines in the right panel mark the overlap region.

This particular measurement is a good example of how the presence of a thin ice cloud affects the polarisation of the scattered light. The off-axis measurement showed strong scattering during the first half of the period and then significantly lower intensities. From the backscattering measurement it was revealed that during the first half the overlap region coincided with an altitude covering the base of an extended cloud layer but later the base was found at higher altitudes. The calculations of the degree of linear polarisation P_L showed a substantial increase, from values below 0.4 to values reaching 0.7, as the signal went from in-cloud scattering to scattering from the relatively cloud free atmosphere (Fig. 19).

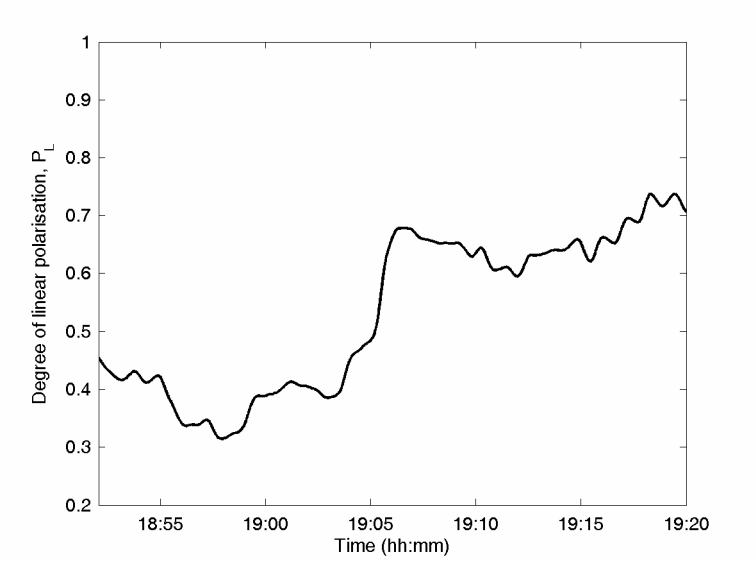

Fig. 19 The degree of linear polarisation of the light scattered from the overlap region shown in Fig. 18. The first half corresponds to scattering from a cloud and the second half scattering from a relatively cloud free atmosphere.

The retrieved polarisation values for the cloud free period in Fig. 18 can be compared with the value obtained from the clear air case on October 19th showed in Fig. 10. The latter measurement was performed during a very stable period without any indication of aerosol layers and resulted in an average polarisation value of 0.70 ± 0.01. This can be compared with the theoretical value for molecular Rayleigh scattering which is 0.98 at the altitude in question (6.35 km). The so-called clear air is cloud free, but the

background aerosol reduces the polarisation of the scattered light. In the presence of clouds the background aerosol contribution to the depolarisation can be neglected. The significant depolarisation introduced by clouds suggests that the cloud particles are in the form of ice, *i.e.* non-spherical. To further confirm this assumption balloon sounding data from Bodø airport, available on the web (http://weather.uwyo.edu/upperair/sounding.html?region=np), was used (Fig. 20).

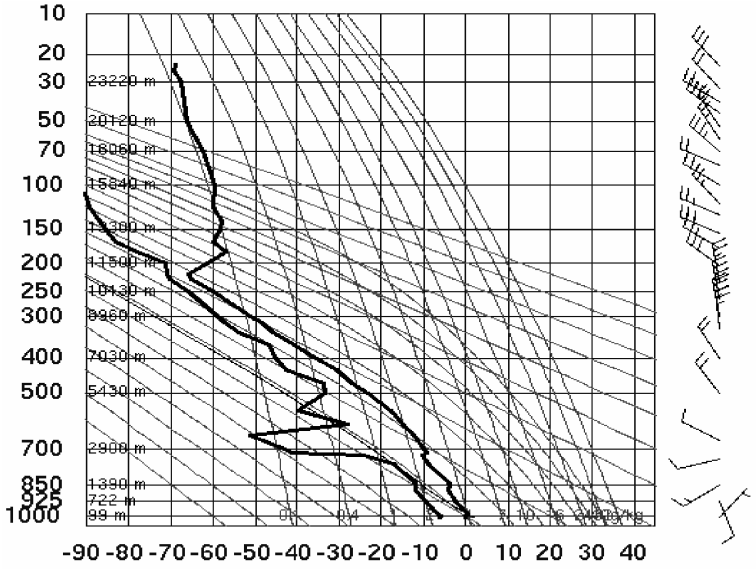

Fig. 20 Data from a balloon sounding performed at Bodø airport 00:00, October 21st, 2006. The temperature profile is given by the right solid black line with temperature in °C on the abscissa and the altitude in m and the pressure in mbar on the ordinate. To the right of the graph wind barbs show the speed and direction of the wind at corresponding altitude. (source: http://weather.uwyo.edu/upperair/sounding.html?region=np)

From the sounding the temperature at the altitude of the overlap region, slightly below 8 km, can be established to around -45 °C. At this temperature close to 100% of the water content can be regarded to be in the form of ice (Rogers & Yau, 1989; Kristjánsson, 2008, private conversation). From the backscatter data a rough estimate of the cloud optical depth, τ_c can be calculated with the formula,

$$\tau_c = -\ln(I_a/I_b) \qquad (21)$$

where I_a and I_b are the averages of the range corrected signals above and below the cloud, respectively. The calculation yields a value of 0.2, which is classified as mildly opaque (Lynch *et al.*, 2002). The optical depths, calculated with Eq. 21, of the clouds investigated in this thesis lie in the range from 0.2 to 0.9 except in one case which showed a value close to 1.4. The influence of multiple scattering can give substantial deviations for the extinction and backscattering coefficients from values based on single scattering. This is true also in the case of optically thin clouds and for second order scattering to be negligible τ_c should be 0.1 or less (Wandinger, 1998). However, for a relative parameter like the depolarisation ratio, such a strict criterion might not be necessary. Reichardt & Reichardt (2003) ran simulations on cirrus clouds and investigated the effect of multiple scattering, up to the order of three, on the depolarisation ratio for perpendicular to parallel polarised light. The ice particles in the simulation were randomly oriented columns and in the case of a cloud with τ_c = 0.6 it was concluded that the difference between the single scattering depolarisation and multiple scattering depolarisation stayed below 1%. The scattering angle in the simulations was 180°. However, as long as the ice particles are randomly oriented and

the variation in polarisation with scattering angle is fairly smooth, as expected for a cloud particle ensemble, the main results from the simulation should be valid also for the CABLE geometry. It is thus concluded that multiple scattering influence on the polarisation results from the studied clouds during the CABLE campaign is limited and that the large depolarisation should be an effect of non-sphericity.

The explanation for the tilted streaks in the light scattering from the cloud, appearing particularly clear in the off-axis data, can be found in the balloon sounding data. From the temperature profile the tropopause height could be found somewhere in the region around 11 km. Below the tropopause the wind barbs reveal that there was a region down to an altitude around 8.5 km with increased northerly wind speed. Above and below that region the wind direction was NW to NNW. This dynamic situation is favourable for the development of wave motions and may be the explanation to the observed structure.

In Fig. 21 a summary of the polarisation values from the measurement during the campaign in October 2006 are summarized. The results are divided into non-cloud and cloud cases, respectively, and show systematically high polarisation for the clear air situation and low polarisation when clouds are present. For the clear air case the P_L values fall in the range from 0.56 ± 0.02 to 0.71 ± 0.04, while the cloud case range from 0.21 ± 0.03 to 0.38 ± 0.04.

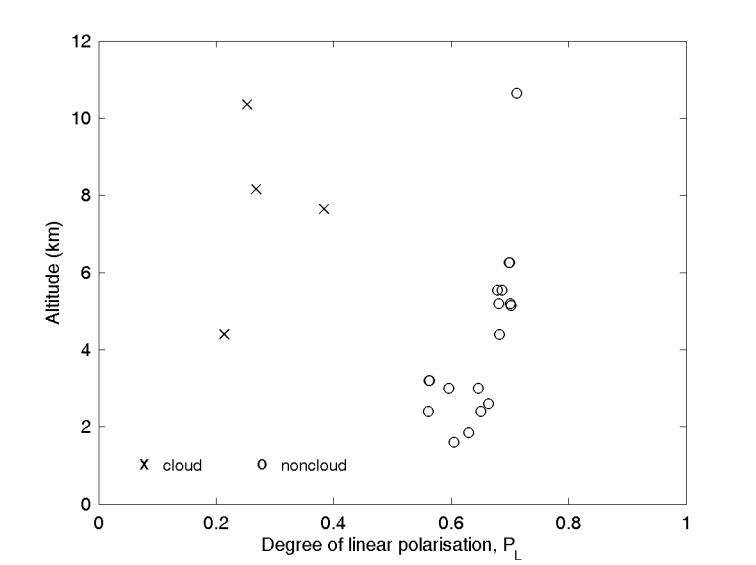

Fig. 21 A summary of the P_L values measured during the CABLE campaign, for cloudy conditions (crosses) and clear air (circles).

5.2.2 Light Scattering Calculations

As described in Chapter 3.1 the phase function shows large variations for scattering from particles with sizes comparable to or larger than the wavelength. If the particles have a finite size distribution width the oscillating pattern becomes less pronounced and as the size distribution grows wider the phase function becomes more and more smoothed. The degree of linear polarisation, P_L shows the same behaviour. This is exemplified in Fig. 22 by the variation in P_L with particle radius and scattering angle for six different size distributions of spherical water droplets (refractive index, m_{532} = 1.33 + 0.00i). The P_L features can be regarded to apply also to spherical ice particles, for which the refractive index, m_{532} = 1.31 + 0.00i, is very close to that for liquid water. The distributions are log-normal and the widths range from σ = 1.00 (monodisperse) to 2.00.

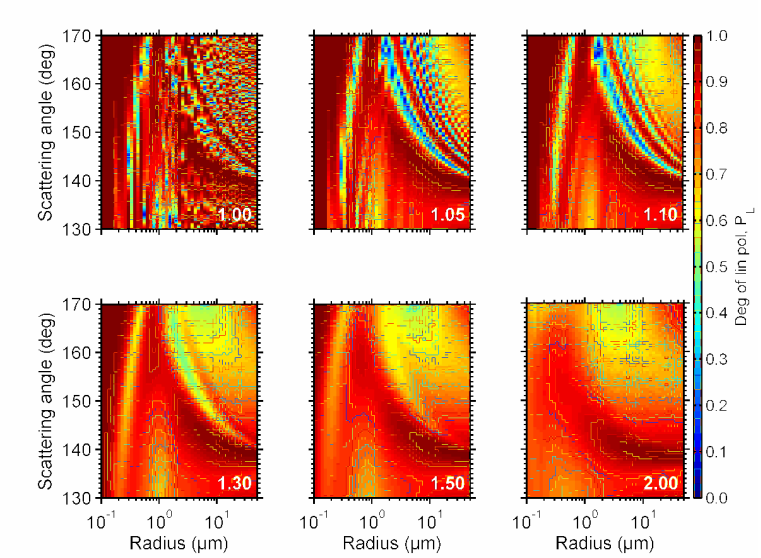

Fig. 22 Degree of linear polarisation as a function of radius and scattering angle. The calculations are performed for spherical water droplets with log-normal size distributions, except in the upper left panel which is for monodisperse droplets. The standard deviations, σ, are indicated in the panels.

The displayed size range is typical for water clouds, which by extensive aircraft observations have been established to consist of spherical droplets with sizes typically ranging from ~1 to 20 µm, as summarized by Liou (1972; 2002). The results in Fig. 22 show that only for very narrow size distributions and scattering angle ranges such low P_L are found. Therefore it may be suspected that the cloud particles studied may have a non-spherical shape, which is the case for ice particles. Since the balloon sounding temperature profiles from Bodø indicated temperatures from -65 to -25 °C, with a majority below -40 °C, at the altitudes of interest it was assumed that most of the studied clouds were of ice type (Rogers & Yau, 1989).

Ice cloud particles are known to take a variety of different geometrical and irregular shapes, such as columns, plates, needles, bullet rosettes, dendrite and aggregates. In cold clouds at high latitudes a large fraction of small crystals has been reported. These tend to be of simple shape like columns and plates, this especially true near the cloud top (Lawson *et al.*, 2001; Liou, 2002; Lynch *et al.*, 2002). To investigate how the shape affect P_L calculations were performed for randomly oriented log-normally distributed cylinders, spheroids and bispheres of ice. The sizes of the particles are expressed as effective radius, *i.e.* the radius of the equal-surface area sphere, according to the

method used by Mishchenko and Travis (1994). The aspect ratios were 1/2, 1 & 2 and 1/2 & 2 for the cylinders and spheroids, respectively. Cylinders with aspect ratio equal to 1 are called compact cylinders. The bispheres were monodisperse with effective radii 1 μm. The P_L curves for the aspherical ice particles are shown in Fig. 23.

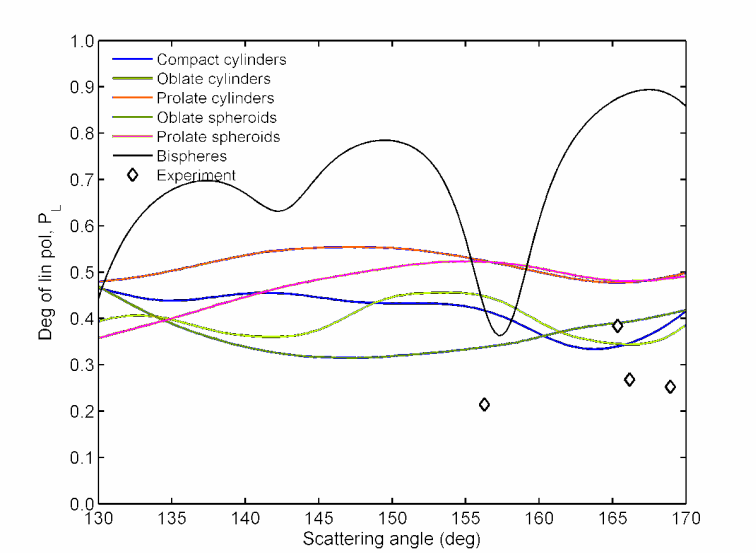

Fig. 23 Degree of linear polarisation as a function of scattering angle. The calculations are performed for log-normal distributions (σ = 1.392) of different randomly oriented aspherical ice particles, ranging from oblate to prolate. Included is also monodisperse bispheres. The diamonds are experimental values obtained from measurements of optically thin clouds.

The calculations reveal that prolates and oblates generally produced values between 0.3 and 0.55, with a tendency for the oblates towards lower polarisation. The monodisperse bispheres are associated with greater variation and generally have higher values. The experimental points have been added to the graph and are marked with diamonds. The values in the range 0.2 – 0.4 still seem hard to explain. In order to stretch the computations to larger radii (max. 7 μm) and slightly larger aspect ratios (1/3 – 3) the particles were set monodisperse and a single scattering angle was examined (Fig. 24). An angle of 165° was chosen since this corresponds to an altitude of 7.8 km ASL, representative for cirrus occurrences during the measurement campaign. The smaller particles show Rayleigh scattering behaviour, *i.e.* $P_L \approx 1$, but at above 30 μm substantial and persistent depolarisation down to values around 0.2 is found. The inset has been added in an effort to show the trend in P_L at around 0.1 μm where the depolarisation seem to increase with asphericity and also according to the pattern, P_L(prolate) < P_L(oblate) < P_L(compact). The obtained results show that the experimentally measured polarisation can be explained with monodisperse ice cylinders larger than 1 μm.

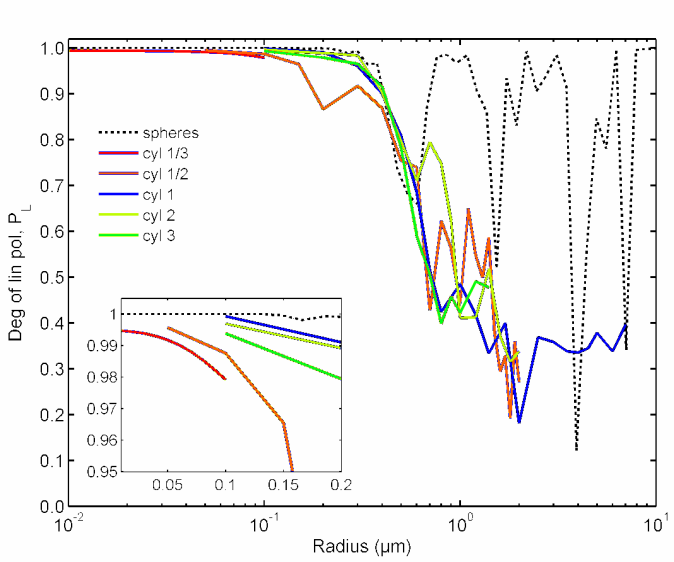

Fig. 24 Trends in degree of linear polarisation for radius and degree of asphericity. The aspect ratio of the cylinders ranges from 1/3 (prolate) to 3 (oblate). The calculations are performed for monodisperse, randomly oriented ice particles at a scattering angle of 165°. Monodisperse spheres are included for comparison. The inset shows the tendency of larger depolarisation for prolates comparing to oblates around 0.1 µm radius.

The simple shapes evaluated in the *T*-matrix calculations could explain the experimental results, but it is likely that ice particles with more complex shapes make a substantial contributions. The particles sizes may also be larger than used in the calculations. To further investigate the effects of particle size, the COPE database (Hess *et al.*, 1998) was used to calculate P_L values for randomly oriented hexagonal ice columns in the size range from 30 to 1300 µm by use of ray-tracing technique. The calculations were performed for particles with minor surface roughness, which has been simulated by assuming a maximum tilt angle of 1° in the calculations (Hess *et al.*, 1998). Figure 25 shows calculated P_L values as a function of scattering angle. The calculated results are qualitatively similar for particles of different dimensions. The polarisation obtained for the hexagonal columns with minor surface roughness are in some cases somewhat higher than the experimental P_L values, indicating that the particles may have more complex structures than the hexagonal columns. One data set marked "rough" instead used a maximum tilt angle of 30°, which simulates extensive surface roughness of the particles. With the combination of the minor and extensive particle roughness reasonably good agreement with the full set of experimental values was accomplished.

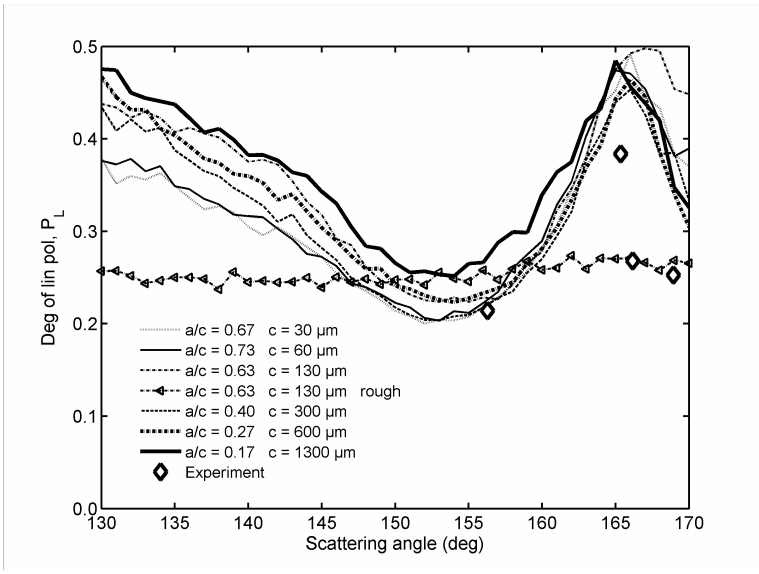

Fig. 25 The degree of linear polarisation determined from cloud experiments (diamonds), and calculated with a geometric optics ray-tracing method for randomly oriented hexagonal columns with different dimensions (lines). *c* is the length of a hexagonal column in µm and *a* is the distance from the center of the column to an edge. The calculations have been performed for ice particles with minor surface roughness, which has been simulated by assuming a maximum tilt angle of 1° in the calculations. One data set (marked rough) instead used a maximum tilt angle of 30°, which simulates extensive surface roughness of the particles.

During the CABLE campaign the degree of linear polarisation was investigated for cloud-free conditions and for measurements where thin and mildly opaque clouds were studied. For the cloud-free conditions P_L values between 0.56 and 0.71 where obtained. The P_L values obtained from the clouds were in the range from 0.21 to 0.38. The degree of linear polarisation calculated from the experiments was compared with light scattering calculations using Lorenz-Mie theory for spherical particles and the *T*-matrix approach for non-spherical rotationally symmetric particles. For particles with sizes of tens of micrometers and larger a geometric optics ray-tracing method was used. It was concluded that the results for cloud-free conditions below 4 km could only be explained by non-spherical particles, while a combination of coarse and fine mode spherical particles could qualitatively reproduce the data at higher altitudes. For the cloud case, calculations for relatively small prolate, oblate and bispherical particles tended give slightly higher values than the experimental. Ray tracing calculations for particles with sizes 30 µm and larger were, however, able to produce some of the experimental values. If a suitable degree of surface roughness was introduced also the remaining experimental P_L values could be obtained.

6 Concluding Remarks and Outlook

In this thesis the construction, development and application of a lidar system has been presented. The system has been employed in two different types of studies. During the early stage the lidar measurements were performed in the city of Göteborg to study the urban aerosol and its development in connection to temperature inversion events. The application proved to be useful for establishment of the boundary layer height and evolution and dispersion of particulate pollutant subsequent to inversion layer break-up. In the next stage the equipment was developed for polarimetric measurements at off-axis scattering angles. These measurements were performed in northern Norway with the aim to study the scattering properties of high latitude cirrus. From the campaigns it can be concluded that the bistatic lidar technique may provide a useful complement to the conventional backscatter lidar.

Strategies for future measurements and developments should be established. First, the data storage time should be substantially reduced in order to get closer to the ultimate time resolution limit set by the laser repetition frequency. The second improvement is to complement the $\lambda/2$ retarder presently used by a $\lambda/4$ retarder in order to obtain the fourth Stokes parameter, V. This also requires an absolute positioning device for the rotating retarder. Last, the implementation of a second remote receiver, or better the possibility to alternate the laser polarisation plane should be offered. This will make it possible to uniquely determine the Müller matrix elements m_{11}, m_{12} and m_{22}, which is explained with the following Stokes parameter-Müller matrix elements relations.

$$
\begin{aligned}
I &= m_{11} + m_{12}\cos 2\psi \\
Q &= m_{12} + m_{22}\cos 2\psi \\
U &= m_{33}\sin 2\psi \\
V &= -m_{34}\sin 2\psi
\end{aligned}
$$

Concerning the measurement strategy, longer measurement series should be collected in order to contribute to the development of improved cirrus cloud climatology and to help validate other techniques being used. Furthermore, the bistatic technique could also be useful for measurements of stratospheric clods.

7 Acknowledgement

Jag skulle vilja tacka:

min handledare Jan Pettersson för uppmuntran, trivsamma diskussioner och all den hjälp jag fått i ”min asymptotiska strävan mot det perfekta”; jag tycker vi har kommit bra överens, av någon anledning verkar du inte ha störts av min grava tidsoptimism

min biträdande handledare Patrik Andersson för mycket, mycket hjälp med det mesta inom mitt doktorerande, men i synnerhet det under alla sena kvällar på lab:et … även om det ibland kunde bli lite otäckt innan vi väl lade locket på

min mentor Georg Witt för att du lärt mig så mycket om ljusspridning, för min nyvunna förmåga att extrahera information, för en tillsynes aldrig sinande ström av historier och anekdoter, rörande såväl fritid som arbete och för alla de oförglömliga äventyr och skojiga upptåg jag fått uppleva i samband med våra mätkampanjer och konferenser

Benny Lönn för de konstruktioner och byggen du presterat trots bristande ritningar

Tomas Hessel för exemplarisk lödning av diverse elektroniska anordningar

Leif Holmlid för lån av oscilloskop och upprepat lån av laserbrillor

personalen på ALOMAR för all hjälp i samband med CABLE-kampanjerna och för trevligt umgänge och nöjesrelaterade skojigheter när jag väl kunnat slita mig från arbetet

Alpo Karppinen för hjälp i samband med datorkrångel

alla på Atmosfärsvetenskap för hjälp, stöd och nöje, särskilt tack vill jag rikta till Helene för korrekturläsning och till Åsa för hjälp med layout-relaterade irritations-moment

före detta kollegor på Fysikalisk kemi goda svunna tiders skull

alla mina vänner som jag faktiskt har kvar trots att det tidvis blivit lite väl mycket inst

8 Bibliography

Bohren, C. F. and Huffman, D. R., *Absorption and scattering of light by small particles*, Wiley Science Paperback Series, New York, 1998

Boy, M., Kulmala, M., Ruuskanen, T. M., Pihlatie, M., Reissell, A., Aalto, P. P., Keronen, P., Dal Maso, M., Hellen, H., Hakola, H., Jansson, R., Hanke, M. and Arnold, F., "Sulphuric acid closure and contribution to nucleation mode particle growth", Atmos. Chem. Phys. **5**, 863-878 (2005)

Dockery, D. W., Pope III, C. A., Xu, X., Spengler, J. D., Ware, J. H., Fay, M. E., Ferris Jr., B. G., Speizer, F. E., "An association between air pollution and mortality in six US cities", New England Journal of Medicine **329**, 1753-1759 (1993)

Fernald, F. G., "Analysis of Atmospheric Lidar Observations: Some Comments", Appl. Opt. **23**, 652-653 (1984)

Fiocco, G. and Grams, G. "Observations of the Aerosol Layer at 20 km by optical Radar", J. Atmos. Sci. **21**, 323-324 (1964)

Fiocco, G. and Smullin, L. D. "Detection of scattering layers in the upper atmosphere (60–140 km) by optical RADAR", Nature **199**, 1275-1276 (1963)

Hess, M., Koelemeijer, R. B. A. and Stammes, P., "COP: a data library of optical properties of hexagonal ice crystals", J. Quant. Spectrosc. Radiat. Transfer **60**, 301-308 (1998)

Heymsfield, A. J., Miller, K. M. and Spinhirne, J. D., "The 27-28 October 1986 FIRE IFO cirrus case study: cloud microstructure", Mon. Weather Rev. **118**, 2313-2328 (1990).

Hinds, W. C., *Aerosol Technology: Properties, Behaviour, and Measurement of Airborne Particles*, John Wiley and Sons, New York, 1999

Holben, B. N., T.F.Eck, I.Slutsker, D.Tanre, J.P.Buis, A.Setzer, E.Vermote, J.A.Reagan, Y.Kaufman, T.Nakajima, F.Lavenu, I.Jankowiak & A.Smirnov, "AERONET - A federated instrument network and data archive for aerosol characterization", *Rem. Sens. Env.*. **66**, (1998)

Holmer, B. and Haeger-Eugensson, M., "Winter land breeze in a high latitude complex coastal area", Phys. Geogr. **20**, 152–172 (1999)

Holmes, N. S., "A review of particle formation events and growth in the atmosphere in the various environments and discussion of mechanistic implications", Atm. Environ. **41**, 2183-2201 (2007)

IPCC, 2007: *Climate Change 2007: The Physical Science Basis. Contribution of Working Group I to the Fourth Assessment Report of the Intergovernmental Panel on Climate Change* [Solomon, S., D. Qin, M. Manning, Z. Chen, M. Marquis, K. B. Averyt, M.Tignor and H. L. Miller (eds.)] Cambridge University Press, Cambridge, United Kingdom and New York, NY, USA, 2007

J. E. Kristjánsson. Department of Geophysics, University of Oslo, Oslo; private conversation

J. T. Twitty, “The inversion of aureole measurements to derive aerosol size distribution,” J. Atmos. Sci. **32**, 584–591 (1974)

Janhäll, S. and Hallquist, M., “A Novel Method for Determination of Size-Resolved, Submicrometer Particle Traffic Emission Factors”, Environ. Sci. Technol. **39**, 7609-7615 (2005)

Janhäll, S., Jonsson, Å. M., Molnàr, P., Svensson, E. A. and Hallquist, M., “Size resolved traffic emission factors of submicrometer particles”, Atm. Environ. **38**, 4331–4340 (2004)

Janhäll, S., Olofson, K. F. G., Andersson, P. U., Pettersson, J. B. C. and Hallquist, M., “Evolution of the urban aerosol during winter temperature inversion episodes”, Atm. Environ. **40**, 5355-5366 (2006)

Kaul, B. V., *Laser Sensing the Aerosol Pollution in the Atmosphere* (dissertation), Institute of Atmospheric Optics, Tomsk, 1977

Klett, J. D., “Stable Analytical Inversion Solution for Processing Lidar Returns”, Appl. Opt. **20**, 211-220 (1981)

Kovalev, V. A. and Eichinger, W. E., *Elastic Lidar: Theory, Practice, and Analysis Methods*, John Wiley &. Sons, Hoboken, 2004

Kulmala, M., Vehkamäki, H., Petäjä, T., Dal Maso, M., Lauri, A., Kerminen, V.-M., Birmili, W., and McMurry, P. H., “Formation and growth rates of ultrafine atmospheric particles: A review of observations”, J. Aerosol Sci. **35**, 143-176 (2004)

Liou, K.-N. and Hansen, J. E., “Intensity and Polarization for Single Scattering by Polydisperse Spheres: A Comparison of Ray Optics and Mie Theory”, J. Atmos. Sci. **28**, 995-1004 (1971)

Liou, K.-N. and Takano, Y., “Interpretation of cirrus cloud polarization measurements from radiative transfer theory”, Geophys. Res. Lett. **29**, 10.1029/2001GL014613 (2002).

Liou, K.-N., “Influence of cirrus clouds on weather and climate processes: A global perspective”, Mon. Weather Rev. **114**, 1167-1199 (1986)

Liou, K.-N., “On Depolarization of Visible Light from Water Clouds for a Monostatic Lidar”, J. Atmos. Sci. **29**, 1000-1003 (1972)

Liou, K.-N., *An Introduction to Atmospheric Radiation*, Academic Press, Amsterdam, 2002

Lynch, D. K., Sassen, K., Starr, D. O’C. and Stephens, G., *Cirrus*, Oxford University Press, New York, 2002

Mace, G. G., Heymsfield, A. J. and Poellot, M. R., “On retrieving the microphysical properties of cirrus clouds using the moments of the millimetre-wavelength Doppler spectrum”, J. Geophys. Res. **107**, (2002)

Matrosov, S. Y., “Variability of Microphysical Parameters in High-Altitude Ice Clouds: Results of the Remote Sensing Method”, J. Appl. Meteorol. **36** (1997)

Mishchenko, M. I. and Sassen, K., "Depolarization of lidar returns by small ice crystals: an application to contrails", Geophys. Res. Lett. **25**, 309-312 (1998).

Mishchenko, M. I. and Travis, L. D., "Light scattering by polydispersions of randomly oriented spheroids with sizes comparable to wavelength of observation", Appl. Opt. **33**, 7206-7225 (1994)

Mishchenko, M. I., Travis, L. D. and Lacis, A. A., *Scattering, absorption and emission of light by small particles*, NASA Goddard Institute for Space Studies, New York, 2005

Mishchenko, M.I. and Travis, L. D., "Capabilities and limitations of a current FORTRAN implementation of the T-matrix method for randomly oriented, rotationally symmetric scatterers", J. Quant. Spectrosc. Radiat. Transfer **60**, 309-324 (1998)

Molnàr, P., Janhäll, S. and Hallquist, M., "Roadside measurements of fine and ultrafine particles at a major road north of Gothenburg", Atm. Environ. **36**, 4115-4123 (2002)

Olofson, K. F. G., Andersson, P. U.,Hallquist, M.,Ljungström, E., Tang, L., Chen, D. and Pettersson, J. B. C., "Urban aerosol evolution and particle formation during wintertime temperature inversions", *accepted for publication in* Atm. Environ. (2008)

Oolman, L., "Univ. Wyoming, Atmospheric soundings," http://weather.uwyo.edu/upperair/sounding.html?region=np

Platnick, S., "NASA, Modis Atmosphere", http://modis-atmos.gsfc.nasa.gov/index.html

Pope III, C. A., Thun, M. J., Namboodiri, M. M., Dockery, D. W., Evans, J. S., Speizer, F. E., Heath Jr., C. W., "Particulate air pollution as a predictor of mortality in a prospective study of US adults", American Journal of Respiratory and Critical Care Medicine **151**, 669-674 (1995)

Pope, C. A. III and Dockery, D. W., "Health Effects of Fine Particulate Air Pollution: Lines that Connect", Journal of the Air and Waste Management Association **56,** 709-742 (2006)

Pope, C. A. III, Burnett, R. T., Thun, M. J., Calle, E. E., Krewski D., Ito, K., Thurston, G. D., "Lung cancer, cardiopulmonary mortality, and long-term exposure to fine particulate air pollution", the journal of the American Medical Association **287**, 1132-1141 (2002)

R. P. Lawson, B.A. Baker, C. G. Schmitt, T. L. and Jensen, J., "An overview of microphysical properties of Arctic clouds observed in May and July 1998 during FIRE ACE", Geophys. Res. **106**, 14989-15014 (2001)

Reichardt, S. and Reichardt, J., "Effect of multiple scattering on depolarization measurements with spaceborne lidars" Appl. Opt. **42** ,3620-6333 (2003)

Rogers, R. R. and Yau, M. K., *A Short Course in Cloud Physics,* Pergamon Press, Oxford, 1989

Seinfeld, J. H. and Pandis, S. N., *Atmospheric chemistry and Physics: From Air Pollution to Climate Change*, John Wiley and Sons, 1998

Stull, R. B., *An Introduction to Boundary Layer Meteorology*, Kluwer Academic Publishers, Dordrecht, 1988

Trepte, C. R., "NASA, CALIPSO" http://www-calipso.larc.nasa.gov/

van de Hulst, H. C., *Light scattering by small particles*, John Wiley & Sons, New York, 1957

Wandinger, U., "Multiple-scattering influence on extinction- and backscatter-coefficient measurements with Raman and high-spectral-resolution lidars", Appl. Opt. **37** ,417-427 (1998)

Ward, G., Cushing, K. M., McPeters, R. D. and Green, A. E. S., "Atmospheric aerosol index of refraction and size-altitude distribution from bistatic laser scattering and solar aureole measurements", Appl. Opt. **12**, 2585-2592 (1973).

Wehner, B., Birmili, W., Gnauk, T. and Wiedensohler, A., "Particle number size distributions in a street canyon and their transformation into the urban-air background: measurements and a simple model study", Atm. Environ. **36**, 2215-2223 (2002)

WHO, 2005 World Health Organisation, *WHO Air quality guidelines global update 2005*, World Health Organisation, Copenhagen, 2005

Witt, G. and Lundin, A., "Laser beam backscatter sounding of the upper atmosphere", MISU Report, AP-2 (1971)

Wylie, D. P., Menzel, W. P., Woolf, H. M. and Strabala, K. I., "Four Years of Global Statistics Using HIRS", J. Climate **7**, 1972-1986 (1994)

Ångström, A., "On the atmospheric transmission of Sun radiation and on dust in the air", Geogr. Ann. **11**, 156– 166 (1929)